

# Anatomy of Eddington-like inversion methods in the context of dark matter searches

Thomas Lacroix, Martin Stref, and Julien Lvalle

Laboratoire Univers et Particules de Montpellier (LUPM),  
Université de Montpellier & CNRS, Place Eugène Bataillon, 34095 Montpellier Cedex 05,  
France

E-mail: [thomas.lacroix@umontpellier.fr](mailto:thomas.lacroix@umontpellier.fr), [martin.stref@umontpellier.fr](mailto:martin.stref@umontpellier.fr),  
[lvalle@in2p3.fr](mailto:lvalle@in2p3.fr)

**Abstract.** Irrespective of the dark matter (DM) candidate, several potentially observable signatures derive from the velocity distribution of DM in halos, in particular in the Milky Way (MW) halo. Examples include direct searches for weakly-interacting massive particles (WIMPs),  $p$ -wave suppressed or Sommerfeld-enhanced annihilation signals, microlensing events of primordial black holes (PBHs), *etc.* Most current predictions are based on the Maxwellian approximation which is not only theoretically inconsistent in bounded systems, but also not supported by cosmological simulations. A more consistent method sometimes used in calculations for direct WIMP searches relies on the so-called Eddington inversion method, which relates the DM phase-space distribution function (DF) to its mass density profile and the total gravitational potential of the system. Originally built upon the isotropy assumption, this method can be extended to anisotropic systems. We investigate these inversion methods in the context of Galactic DM searches, motivated by the fact that the MW is a strongly constrained system, and should be even more so with the ongoing Gaia survey. We still draw conclusions that apply to the general case. In particular, we illustrate how neglecting the radial boundary of the DM halo leads to theoretical inconsistencies. We also show that several realistic configurations of the DM halo and the MW baryonic content entail ill-defined DFs, significantly restricting the configuration space over which these inversion methods can apply. We propose consistent solutions to these issues. Finally, we compute several observables inferred from constrained Galactic mass models relevant to DM searches (WIMPs or PBHs), *e.g.* moments and inverse moments of the DM speed and relative speed distributions.

---

## Contents

<b>1</b>	<b>Introduction</b>	<b>1</b>
<b>2</b>	<b>Eddington’s inversion method and its anisotropic extensions</b>	<b>3</b>
2.1	Jeans’ theorem and spherical systems	3
2.2	Eddington’s inversion for an isotropic system	5
2.3	Anisotropic extensions	6
2.3.1	Constant anisotropy	7
2.3.2	Osipkov-Merritt model	8
2.3.3	Other possibilities	9
2.4	Beyond spherical symmetry	10
<b>3</b>	<b>Some issues of the Eddington formalism</b>	<b>10</b>
3.1	Radial-boundary-induced divergence, the escape speed, and some regularization procedures	11
3.1.1	Characterization of the spatial-boundary-induced divergence	11
3.1.2	Regularization through the density profile	14
3.1.3	Regularization through the phase-space distribution	16
3.1.4	Regularization of the boundary-induced divergence: Summary	18
3.2	Positivity and stability issues	19
3.2.1	Positive distribution functions	20
3.2.2	Stable distribution functions	21
3.2.3	Positive and stable distribution functions: summary	25
<b>4</b>	<b>Impact on predictions for dark matter searches</b>	<b>26</b>
4.1	Direct-search-like observables	27
4.2	Indirect-search-like observables	29
<b>5</b>	<b>Conclusion</b>	<b>32</b>
<b>A</b>	<b>Galactic mass models used in this study</b>	<b>36</b>
<b>B</b>	<b>Relative velocity distribution function</b>	<b>37</b>
B.1	Isotropic system	38
B.2	Anisotropic extensions	39

---

## 1 Introduction

The tremendous progress made on both direct and indirect particle dark matter (DM) searches over the past few decades has yielded an incredible wealth of data, calling for predictions as reliable as possible in order to draw robust conclusions on models (see reviews on DM models and search strategies in *e.g.* Refs. [1–10]). Galactic DM searches are among the most promising because the Milky Way (MW) is a local and constrained system. However, most associated theoretical predictions are still based on simplifying assumptions for the DM distributions in real space and/or phase space, despite regular improvements in

modeling techniques and observational constraints. Therefore, it is usually difficult to figure out the level of uncertainties associated with these assumptions. The fact that different studies use different assumptions makes it even more difficult to self-consistently exploit the genuine complementarity between the constraints or discovery avenues, which now becomes crucial as experiments have started to probe significant parts of the parameter space allowed for popular particle DM scenarios. It is worth emphasizing that designing constrained and theoretically sound models for the DM distribution in real space and phase space in target systems is crucial for any astrophysical DM search, irrespective of the DM scenario.

The Gaia mission [11, 12] is currently shedding new and unprecedented light on the distribution of DM in the Milky Way (MW), complementary to other stellar surveys (see *e.g.* Refs. [13, 14]). The Gaia data will increase the accuracy in predictions of DM-related observables, provided reliable methods ensure their use in a sensible way. The overall challenge is to better control not only the spatial distribution of DM, but also its full phase-space distribution function (DF henceforth), which are the major sources of uncertainties in predictions for DM searches. This will likely not be an easy task [15], and there is room for significant theoretical improvement over the techniques currently used in DM searches. The phase-space DF enters the calculations of many important DM-related observables that depend directly on the DM velocity distribution—for example the direct DM detection rate, averaged  $p$ -wave-suppressed or Sommerfeld-enhanced annihilation cross sections, the microlensing event rate of compact DM objects, *etc.* Moreover, since the spatial distribution of DM is the integral of the phase-space DF over momentum space, it is clear that a common framework is necessary to make self-consistent comparisons between direct and indirect Galactic DM searches in the broad sense, as both should exhibit some correlations (largely ignored so far, except in a few studies, *e.g.* Ref. [16]).

In this paper, we wish to investigate the status of some theoretical approaches that attempt to self-consistently predict the DM phase-space DF from the full content of the target system by virtue of the (steady-state) Boltzmann equation, the Jeans theorem, and the Poisson equation, *i.e.* from first principles—we will place ourselves in the context of collisionless cold DM from now on. These methods go beyond the simplistic approximation of a Maxwell-Boltzmann distribution, well suited to get fast order-of-magnitude estimates, but known for long not to apply to bounded systems [17], and not to comply with dynamical constraints on the MW. These methods are complementary to data-driven approaches (*e.g.* Ref. [18]). Other approaches rely on fits from hydrodynamic cosmological simulations, but except for the essential physical insight provided by generic features found in simulations (*e.g.* Refs. [19, 20]), the blind extrapolation of these fits to describe a single, specific, and constrained object like the MW is questionable; not to mention the uncertainties induced by the empirical assumptions in the description of baryonic effects and by the limited resolution. Cosmological simulations are still very important tools to test prediction methods as they provide a framework in which all the gravitational constituents are dynamically correlated [21].

A well-known example and *a priori* self-consistent phase-space DF prediction from the gravitational system content is the so-called Eddington inversion method [22] (and its anisotropic extensions, like the Osipkov-Merritt models [23, 24]), which we discuss extensively in this paper. This approach has already been used in the context of direct particle DM searches (see *e.g.* Refs. [25–32]), as well as indirect searches (see *e.g.* Refs. [33–36]). A net benefit from this method is that it can make use of evolved and constrained Galactic mass models (*e.g.* Refs. [14, 37–39]), providing a much more sensible theoretical description

of the phase space. However, its validity range has not been studied in detail in the context of DM searches, especially in a complex system like the MW, whose gravitational potential is dominated by the baryons in the central regions. In this work, we will show that it actually cannot apply to all DM-baryon pair configurations, leading to ill-defined phase-space DFs even for rather conventional Galactic mass models. This is the manifestation of gravitationally unstable DFs, and of the fact that some degrees of freedom are missing to fully describe the system. We carefully delineate the DM-baryon parameter space where the Eddington-like calculations may apply. We also discuss several other theoretical issues that have been overlooked in the literature, such as the impact of the radial boundary of the system, which should not be neglected to guarantee the existence of a closed system of equations, but may in turn induce divergences in the velocity distribution. We propose ways to circumvent these issues, and provide results for some observables specific to DM searches in the framework of the Galactic mass model of Ref. [39] (see App. A), namely radial profiles of the moments of the DM speed (direct DM searches, microlensing event rate for compact DM objects, *etc.*) and of the (two-body) relative DM speed ( $p$ -wave-suppressed and Sommerfeld-enhanced annihilation) distributions. We stress that although we focus on the MW in this paper, the general aspects of this study are still relevant to the use of the Eddington formalism to describe the DM phase-space DF of any other bounded system (with or without baryons). We also emphasize that this study focuses on the theoretical self-consistency of the formalism itself, which is a first important step with, as we will see, quantitative consequences. It is very likely that several assumptions inherent to this theoretical description, like steady state, spherical symmetry, or the fact that potential effects coming from large substructures or recent mergers are neglected (*e.g.* the Large or Small Magellanic Cloud), will break down at some level, inducing another layer of systematic uncertainties. However, more detailed comparisons between the theoretical errors addressed here and other systematic uncertainties are left to a forthcoming dedicated paper[21].<sup>1</sup>

The paper is organized as follows. In Sec. 2, we review the Eddington-inversion formalism and some of its anisotropic extensions. In Sec. 3, we explain in detail the issues mentioned above and their physical consequences—the divergences induced by the radial boundary and the inability of the formalism to describe some DM-baryon configurations allowed by kinematic constraints. In that section, we discuss some possible ways out that allow one to recover a self-consistent description of the phase space. In Sec. 4, we illustrate our results by calculating a series of observables relevant to particle DM direct and indirect searches. These results can be straightforwardly used for predictions in these fields. Finally, we conclude in Sec. 5.

## 2 Eddington’s inversion method and its anisotropic extensions

In this section, we review the basic concepts that will be useful throughout the discussion. Though mostly reviewing standard knowledge [40], we will also point out several technical details that are often overlooked or unclear in the literature.

### 2.1 Jeans’ theorem and spherical systems

The Jeans theorem states that any steady-state solution of the collisionless Boltzmann equation can be written as a function of isolating integrals of motion [40, 41]. In the particular

---

<sup>1</sup>Preliminary results based on tests on hydrodynamic cosmological simulations show that, surprisingly enough, the formalism performs rather well on “Milky Way-like” virtual galaxies.

case of a system with spherical symmetry, the energy and the modulus of the angular momentum are such integrals of motion. Consequently, the phase-space DF of such a system can be written  $f(\vec{r}, \vec{v}) \equiv f(\mathcal{E}, L)$ , where  $L = |\vec{r} \times \vec{v}|$  is the modulus of the angular momentum per unit mass, and

$$\mathcal{E} = \Psi(r) - \frac{v^2}{2} \quad (2.1)$$

is the relative energy per unit mass—we assume all the DM particles in the system to be identical. In Eq. (2.1),  $v$  is the velocity, and

$$\Psi(r) = \Phi_0 - \Phi(r) \quad (2.2)$$

is the (positive-definite) relative gravitational potential, where  $\Phi(r)$  is the solution to Poisson’s equation going to 0 at infinity. The constant  $\Phi_0$  is the value of  $\Phi(r)$  at some reference radius—usually taken to be the physical boundary of the system—called  $R_{\max}$  in the following. This ensures that the potential is positive-definite over the system except at the boundary where it vanishes. It will sometimes prove convenient to distinguish the baryonic ( $\Psi_B$ ) and DM ( $\Psi_D$ ) contributions to the potential that we introduce here through the following equation,

$$\Psi(r) = \Psi_D(r) + \Psi_B(r). \quad (2.3)$$

For the full system or for each component, and provided the mass profile or the density profile are known, the relative potential  $\Psi$  can be related to the mass distribution of the system (or its individual components) through Poisson’s equation, and reads

$$\Psi(r) = \int_r^{R_{\max}} dr' \frac{Gm(r')}{r'^2}, \quad (2.4)$$

where the mass inside the sphere of radius  $r$  is related to the mass density  $\rho$  through

$$m(r) = 4\pi \int_0^r dr' \rho(r') r'^2. \quad (2.5)$$

Like for the potential, the mass can be split into several components, *e.g.* a baryonic component ( $m_B$ ) and a DM one ( $m_D$ ). We stress that the DM potential  $\Psi_D$  can be calculated from Eq. (2.4) only when the DM content is specified from its density profile  $\rho$ ; we will see later that in some cases, we can only self-consistently get the potential from the DF, where the radial coordinate  $r$  only emerges by solving the Poisson equation given below in Eq. (2.9). In contrast, the baryonic potential will invariably be defined from Eq. (2.4) from now on.

We limit our study to systems with spherical symmetry, therefore when dealing with a non-spherical density component  $\rho(\vec{x})$  (*e.g.* baryons which often have an approximate axial symmetry in galaxies) we compute the corresponding mass inside a radius  $r$  via

$$m(r) = \int_{|\vec{x}| \leq r} d^3\vec{x} \rho(\vec{x}), \quad (2.6)$$

and its “spherically symmetrized potential” using Eq. (2.4). This approximation can be relaxed in principle, though the consistent treatment of an axisymmetric distribution is much more involved (see Sec. 2.4). In the following, all non-spherical components such as the bulge

and disks in the model of Ref. [39] (see App. A), will be “spherically symmetrized” relying on Eq. (2.6).

The DF is therefore related to the mass density via

$$\rho(r) = \int d^3\vec{v} f(r, \vec{v}) = \int d^3\vec{v} f(\mathcal{E}, L). \quad (2.7)$$

Note that in Eq. (2.7), the DF is normalized to the total mass of the component of interest. We keep this convention in the following. We can further define the velocity distribution  $f_{\vec{v}}$  and the speed distribution  $f_v$  as follows:

$$f_{\vec{v}}(\vec{v}, r) \equiv \frac{f(\mathcal{E}, L)}{\rho(r)} \quad (2.8a)$$

$$f_v(|\vec{v}|, r) \equiv v^2 \int d\Omega_v f_{\vec{v}}(\vec{v}, r), \quad (2.8b)$$

where  $d\Omega_v$  encodes the angular content of the velocity distribution. From the above definition, both  $f_{\vec{v}}$  and  $f_v$  carry the usual units and are normalized to unity. We stress that the DF introduced in Eq. (2.7) is implicitly assumed to further satisfy Poisson’s equation

$$\Delta\Psi_i = -4\pi G \rho_i(r) = -4\pi G \int d^3\vec{v} f_i(\mathcal{E}, L) = -4\pi G \int_0^\Psi d\mathcal{E}' \sqrt{2(\Psi - \mathcal{E}')} f_i(\mathcal{E}', L), \quad (2.9)$$

which will turn out to be important later on. When  $\rho_i(r)$  is specified, the above equation reduces to Eq. (2.4) if the boundary condition  $\Psi_i(R_{\max}) = 0$  is considered (here, this will always be the case for the baryonic component). Otherwise, Eq. (2.9) will have to be solved explicitly to compute the potential. The  $i$  index makes it clear that although the energy  $\mathcal{E}$  depends on the full potential  $\Psi = \sum_i \Psi_i$  and thereby on all the gravitational components of the system, the Poisson equation only relates the individual components to their own phase-space DF.

There is no general classification of the solutions of the collisionless Boltzmann equation. Therefore, further assumptions on the properties of the phase space are needed. In the following, we recall the main equations of the Eddington inversion formalism—which allows one to derive a phase-space DF for a given galactic mass model and for particular assumptions on the anisotropy of the system—before discussing in detail theoretical issues that may arise from the method.

## 2.2 Eddington’s inversion for an isotropic system

We first set about describing the simplest case of a spherically symmetric and isotropic DM distribution. In that case, the angular momentum is irrelevant, and the dependence of the DF on integrals of motion simplifies to an energy dependence,  $f \equiv f(\mathcal{E})$ . Such a DF is referred to as ergodic. Using Eq. (2.1) as a change of variables to eliminate the velocity, we can rewrite Eq. (2.7) as

$$\rho(r) = 4\pi\sqrt{2} \int_0^{\Psi(r)} f(\mathcal{E}) \sqrt{\Psi(r) - \mathcal{E}} d\mathcal{E}. \quad (2.10)$$

Note that we only consider *self-gravitating* systems, which means all particles in the system are gravitationally bound to it and have  $\mathcal{E} \geq 0$ . As a result,  $f(\mathcal{E} < 0) = 0$ . This translates

into a lower bound of  $\mathcal{E} = 0$  in the integral in Eq. (2.10). For general systems that are not self-gravitating, the lower bound would be  $\mathcal{E} = -\infty$ .

Since  $\Psi$  is a monotonically decreasing function of  $r$  in a realistic stationary system, one can define  $\rho$  as a function of  $\Psi$  instead of  $r$ . Differentiating Eq. (2.10) with respect to  $\Psi$ , one obtains

$$\frac{d\rho}{d\Psi} = \sqrt{8\pi} \int_0^\Psi \frac{f(\mathcal{E})}{\sqrt{\Psi - \mathcal{E}}} d\mathcal{E}. \quad (2.11)$$

This is an Abel equation, which can be inverted to give Eddington's formula [22, 40]:

$$f(\mathcal{E}) = \frac{1}{\sqrt{8\pi^2}} \frac{d}{d\mathcal{E}} \int_0^\mathcal{E} \frac{d\Psi}{\sqrt{\mathcal{E} - \Psi}} \frac{d\rho}{d\Psi}. \quad (2.12)$$

A more convenient form of Eddington's formula that does not explicitly feature a derivative with respect to  $\mathcal{E}$  can be obtained after integrating by parts:

$$\begin{aligned} f(\mathcal{E}) = & \frac{1}{\sqrt{8\pi^2}} \left\{ \frac{1}{\sqrt{\mathcal{E}}} \left[ \frac{d\rho}{d\Psi} \right]_{\Psi=0} + \int_0^\mathcal{E} \frac{d\Psi}{\sqrt{\mathcal{E} - \Psi}} \frac{d^2\rho}{d\Psi^2} \right\} \\ & \left[ = \frac{2}{\sqrt{8\pi^2}} \left\{ \frac{1}{2\sqrt{\mathcal{E}}} \left[ \frac{d\rho}{d\Psi} \right]_{\Psi=0} + \sqrt{\mathcal{E}} \left[ \frac{d^2\rho}{d\Psi^2} \right]_{\Psi=0} + \int_0^\mathcal{E} d\Psi \sqrt{\mathcal{E} - \Psi} \frac{d^3\rho}{d\Psi^3} \right\} \right]. \end{aligned} \quad (2.13)$$

This is the form we will use and discuss extensively in the following (the last line in brackets corresponds to an additional integration by parts, which will prove insightful later on). Integrating Eq. (2.11), one can reconstruct the density profile from the DF:

$$\rho(\Psi) = \rho(\Psi = 0) + 4\pi\sqrt{2} \int_0^\Psi d\mathcal{E} \sqrt{\Psi - \mathcal{E}} f(\mathcal{E}), \quad (2.14)$$

where  $\rho(\Psi = 0) = \rho(r = R_{\max})$  is the density at the boundary of the system, very often neglected in the literature whereas it is an important ingredient to test the self-consistency of the chain of calculations (one must obviously recover the initial input density profile from integrating the DF). Indeed, the Abel inversion is performed on  $d\rho/d\Psi$  rather than  $\rho$ . We also emphasize the importance of the term  $\propto 1/\sqrt{\mathcal{E}}$  in Eq. (2.13) to get a consistent reconstruction of  $\rho$  up to the radial boundary  $R_{\max}$  of the system, except in the special limit  $R_{\max} \rightarrow \infty$ . As a potentially important technical consequence, the self-consistent normalization of the velocity or speed distributions  $f_{\bar{v}/v}$  defined in Eq. (2.8) is no longer guaranteed—neglecting the term  $\propto 1/\sqrt{\mathcal{E}}$  therefore imposes to normalize the distributions  $f_{\bar{v}/v}$  by hand. An illustration is presented in Fig. 1, where the dashed curves show the reconstructed profiles when neglecting  $\rho(\Psi = 0)$ , the dotted curves further neglect the term of the DF  $\propto 1/\sqrt{\mathcal{E}}$ , all compared with the fully reconstructed profiles (solid lines).

As a side remark, note that  $\rho$  and  $\Psi$  need not be related for the Eddington inversion to work. For instance, if the system contains DM and baryons,  $\rho$  refers to the DM density, whereas  $\Psi = \Psi_D + \Psi_B$  is the total potential. In that case,  $\Psi$  cannot be determined from the sole knowledge of the DM density. That  $\rho$  and  $\Psi$  can be independent will have consequences in terms of physical self-consistency of the derived DF, as will be discussed in Sec. 3.2.

### 2.3 Anisotropic extensions

When the system features some degree of anisotropy, the density profile and the total gravitational potential are no longer sufficient to determine the DF because the angular momentum

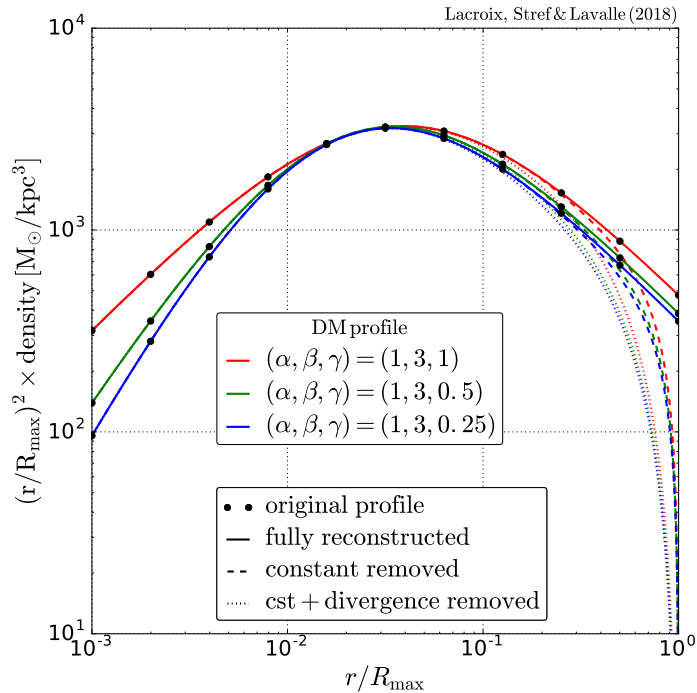


**Figure 1:** Initial density profiles with different inner slopes  $\gamma = 0.25, 0.5, 1$  (see App. A) taken from Ref. [39] and their reconstruction from Eq. (2.14). The black circles show the original profiles, the solid lines the full reconstructions based on Eq. (2.14), the dashed lines neglect the constant term of Eq. (2.14), and the dotted lines neglect both the latter and the  $1/\sqrt{\mathcal{E}}$  term in the calculation of the DF  $f(\mathcal{E})$  [see Eq. (2.13) and Sec. 3.1].

$\vec{L}$  enters the game, and an ansatz for  $f(\mathcal{E}, \vec{L})$  is required to account for the dependence of the DF on these new degrees of freedom—for the spherically symmetric systems considered here, the phase space is only extended by the modulus  $|\vec{L}| = L$ . An anisotropic system is usually characterized in terms of an anisotropy parameter [42]:

$$\beta(r) = 1 - \frac{\sigma_\theta^2 + \sigma_\phi^2}{2\sigma_r^2}, \quad (2.15)$$

where  $\sigma_r$ ,  $\sigma_\theta$  and  $\sigma_\phi$  are the velocity dispersions in spherical coordinates. If orbits in the system of interest are mostly tangential, we have  $\sigma_r^2 \ll \sigma_\theta^2 + \sigma_\phi^2$  and  $\beta < 0$ ,  $|\beta| \gg 1$ . If orbits are mostly radial, we get  $\sigma_r^2 \gg \sigma_\theta^2 + \sigma_\phi^2$  and  $\beta = 1$ . In the following, we describe two simple ansätze that provide semi-analytical solutions from the Abel inversion procedure in the anisotropic case, and briefly discuss more sophisticated approaches.

### 2.3.1 Constant anisotropy

A simple extension of the Eddington method deals with systems having a constant anisotropy parameter  $\beta(r) = \beta_0$ . The simplest ansatz for the DF that separates the effects of energy and angular momentum takes the following form [40, 43, 44]:

$$f_{\beta_0}(\mathcal{E}, L) = G(\mathcal{E})L^{-2\beta_0}. \quad (2.16)$$



The function  $G$  is related to the density profile through

$$\chi \equiv r^{2\beta_0} \rho = \lambda(\beta_0) \int_0^\Psi G(\mathcal{E}) (\Psi - \mathcal{E})^{\frac{1}{2}-\beta_0} d\mathcal{E}, \quad (2.17)$$

where

$$\lambda(\beta_0) = 2^{\frac{3}{2}-\beta_0} \pi^{\frac{3}{2}} \frac{\Gamma(1-\beta_0)}{\Gamma(3/2-\beta_0)}, \quad (2.18)$$

where  $\Gamma$  is the Gamma function (Euler integral of the second kind). This leads to the Abel equation

$$\frac{d^n \chi}{d\Psi^n} = \lambda(\beta_0) \left(\frac{1}{2} - \beta_0\right)! \int_0^\Psi G(\mathcal{E}) (\Psi - \mathcal{E})^{\frac{1}{2}-\beta_0-n} d\mathcal{E}, \quad (2.19)$$

where

$$\left(\frac{1}{2} - \beta_0\right)! \equiv \begin{cases} \left(\frac{1}{2} - \beta_0\right) \dots \left(\frac{1}{2} - \beta_0 - (n-1)\right) & \text{for } \beta_0 < \frac{1}{2} \\ 1 & \text{for } \frac{1}{2} \leq \beta_0 < 1 \end{cases}, \quad (2.20)$$

and

$$n = \left\lfloor \frac{3}{2} - \beta_0 \right\rfloor, \quad (2.21)$$

with  $\lfloor x \rfloor$  the floor of  $x$ . The solution of this equation can be expressed as

$$G(\mathcal{E}) = \frac{\sin((n-1/2+\beta_0)\pi)}{\pi \lambda(\beta_0) (1/2-\beta_0)!} \frac{d}{d\mathcal{E}} \int_0^\mathcal{E} d\Psi \frac{d^n \chi}{d\Psi^n} (\mathcal{E} - \Psi)^{n-3/2+\beta_0}, \quad (2.22)$$

We note that in the isotropic limit  $\beta_0 \rightarrow 0$ , the expression of  $G$  in Eq. (2.22) boils down to the Eddington DF given in Eq. (2.12) as expected. If  $\beta_0$  is a half-integer, the integral in Eq. (2.22) boils down to a derivative [45]. This allows one to analytically express the DF of any system with a half-integer anisotropy [46].

### 2.3.2 Osipkov-Merritt model

Another extension of the Eddington formalism is the Osipkov-Merritt DF [23, 24] which describes a system where the anisotropy parameter is no longer constant, but takes the following radial dependence:

$$\beta(r) = \frac{r^2}{r^2 + r_a^2}, \quad (2.23)$$

where  $r_a$  is a free parameter referred to as the anisotropy radius. This model is isotropic in the inner regions  $r \ll r_a$ , while it exhibits a full radial anisotropy in regions  $r \gg r_a$ . It cannot describe tangential anisotropy. The full isotropic case is recovered in the limit  $r_a \rightarrow \infty$ . This expression is derived by assuming that the DF no longer factorizes out its dependence on energy and angular momentum, but mixes them through a variable  $Q$ ,

$$f(\mathcal{E}, L) = f_{\text{OM}}(Q), \quad (2.24)$$

where  $Q = \mathcal{E} - \frac{L^2}{2r_a^2}$ . By solving

$$\rho(r) = \int d^3\vec{v} f_{\text{OM}}(Q), \quad (2.25)$$

one readily obtains

$$\rho(r) = \frac{r_a^2}{r^2 + r_a^2} \rho_{\text{OM}}(r), \quad (2.26)$$

where

$$\rho_{\text{OM}}(r) = \rho_{\text{OM}}(\Psi(r)) = 4\pi\sqrt{2} \int_0^\Psi f_{\text{OM}}(Q) \sqrt{\Psi - Q} dQ. \quad (2.27)$$

The Abel equation is then

$$\frac{d\rho_{\text{OM}}}{d\Psi} = \sqrt{8\pi} \int_0^\Psi \frac{f_{\text{OM}}}{\sqrt{\Psi - Q}} dQ, \quad (2.28)$$

and its solution

$$f_{\text{OM}}(Q) = \frac{1}{\sqrt{8\pi^2}} \frac{d}{dQ} \int_0^Q \frac{d\Psi}{\sqrt{Q - \Psi}} \frac{d\rho_{\text{OM}}}{d\Psi}. \quad (2.29)$$

The expression of  $f_{\text{OM}}$  is identical to that of the standard Eddington DF in Eq. (2.13) when  $Q$  and  $\rho_{\text{OM}}$  are identified with  $\mathcal{E}$  and  $\rho$ , respectively (in the isotropic limit  $r_a \rightarrow \infty$ , both expressions match).

### 2.3.3 Other possibilities

The two methods discussed above are the simplest ones accounting for anisotropy in the velocity distribution, as they depend only on one free parameter ( $\beta_0$  or  $r_a$ ). Other DFs involving more free parameters can be found in the literature, such as a straightforward generalization of both constant anisotropy and Osipkov-Merritt models [45],

$$f(\mathcal{E}, L) = G(Q) L^{-2\beta_0}. \quad (2.30)$$

Motivated by the anisotropy profiles  $\beta(r)$  observed in N-body simulations, some authors have also considered linear combinations of the constant anisotropy DF and the Osipkov-Merritt DF [30]

$$f(\mathcal{E}, L) = w f_{\text{OM}}(Q) + (1 - w) G(\mathcal{E}) L^{-2\beta_0}, \quad (2.31)$$

while others have looked at different functional forms [47]:

$$f(\mathcal{E}, L) = F(\mathcal{E}) \left(1 + \frac{L^2}{2L_0^2}\right)^{-\beta_\infty + \beta_0} L^{-2\beta_0}. \quad (2.32)$$

Models of Refs. [30, 47] both contain a set of three free parameters ( $\{w, r_a, \beta_0\}$  or  $\{L_0, \beta_0, \beta_\infty\}$ ) calibrated on simulations. Irrespective of the different proposals to cope with anisotropy in the DM velocity field, we stress that the latter is still hardly constrained by kinematic observations of visible matter.

## 2.4 Beyond spherical symmetry

In this study, we will not go beyond spherical symmetry except to approximately integrate the effects of some non-spherical components like the baryonic bulge and disks [see Eq. (2.6) and discussion below]. Here, for the sake of completeness, we just review some more involved theoretical methods that can be used to cope with this delicate problem. When dealing with a system that is not spherically symmetric, the energy and the angular momentum might not be the most convenient variables to work with. The authors of Refs. [40, 48] promote instead the *angle-action* variables as a phase-space coordinate system. The components of the action vector  $\vec{J}$  are integrals of motion and the angle vector  $\vec{\Theta}$  is the Hamiltonian conjugate of  $\vec{J}$ . A crucial property of the actions is their constancy in a slowly varying potential. In such a potential, a DF of the form  $f(\vec{J})$  is then also a constant. This property was used as a starting point in Ref. [49] to compute a phase-space model of the Milky Way, assuming baryons are slowly accreted onto an initially spherical dark halo. This led, in this theoretical framework, to the exclusion of an adiabatic compression of the dark halo [50], favoring instead heating at its center and the presence of a  $\sim 2$  kpc core [51] in agreement with a detailed study of the bar/bulge dynamics [52].

The philosophy behind this technique is opposite to Eddington's since here the starting point is the DF, from which the potential is computed through an iterative procedure, while in the Eddington case one starts with the potential and the density and derives the DF from there. Just like there is a lot of freedom when choosing the functional form of the DF in the anisotropic extensions of the Eddington inversion method, there is also some freedom in choosing the functional form of the action-dependent DF. Assumptions must therefore be made on its dependency with respect to each action and this may introduce theoretical uncertainties in the calculation which are difficult to evaluate. Nevertheless, this method constitutes the state of the art of Galactic phase-space modeling and it captures details beyond the reach of the Eddington formalism.

This level of detail might not be required in the context of DM searches though, as one is mostly interested in evaluating the astrophysical uncertainties relevant to complementary observables of interest in a self-consistent framework. The Eddington formalism actually provides such a framework, while being in practice more flexible than the angle-action approach. Moreover, global dynamical constraints are easier to account for in the Eddington approach from a technical point of view. However, as we will show in the following, the Eddington inversion is not a self-regulated approach as it does not prevent from getting unstable or ill-defined phase-space configurations, whereas action-angle methods are a priori immune to these defects. It is therefore important to delineate as rigorously as possible the domain of application of the Eddington inversion. Ultimately, more systematic comparisons with action-angle methods should help further reduce the theoretical uncertainties and provide complementary understanding of the potential failures of the Eddington inversion, but this goes beyond the scope of this paper.

## 3 Some issues of the Eddington formalism

In this section, we discuss in detail two issues that we have identified in the Eddington inversion method, and which have been overlooked in the literature focused on DM searches. The first one concerns the impact of the spatial boundary of the dark halo, which is usually neglected while this leads to theoretical inconsistency and also potentially to mistreatments

of the tail of the DM velocity distribution. The second one is related to the fact that some perfectly licit DM-baryons configurations may actually lead to unstable DFs.

We recall that the main benefits of the Eddington formalism (including its anisotropic extensions) in the context of DM searches is precisely to provide a self-consistent and constrained framework to compute both density-dependent and velocity-dependent observables. A noticeable strength is to be able to use a kinematically constrained Galactic mass model and self-consistently propagate the associated uncertainties to the DM observables. However, the two issues mentioned above and further detailed in this section jeopardize this possibility.

In the following, all concrete calculations of the DFs will be made using the best-fit Galactic mass models of Ref. [39] (McM17 models henceforth), unless specified otherwise. The nominal model is featured by an NFW DM halo and a baryonic component made of a stellar bulge, stellar disks, and gaseous disks, all of these components being constrained from recent kinematic data. The parameters of these models are summarized in App. A.

### 3.1 Radial-boundary-induced divergence, the escape speed, and some regularization procedures

#### 3.1.1 Characterization of the spatial-boundary-induced divergence

A generic issue with the Eddington DF is the presence of a divergence in the limit  $\mathcal{E} \rightarrow 0$  due to the term  $(d\rho/d\Psi)_{\Psi=0} \times 1/\sqrt{\mathcal{E}}$  present in Eq. (2.13). This derivative is evaluated at the radial boundary of the system and does not vanish for conventional halo profiles, unless the boundary is sent to infinity. However, this boundary must be finite just because of the presence of neighboring galaxies. It is precisely what allows us to make a realistic interpretation of an escape speed, which has some impact on *e.g.* direct searches of low-mass WIMPs [32].

This diverging term  $\propto 1/\sqrt{\mathcal{E}}$  is actually very often dropped without deep justifications. However, this jeopardizes the self-consistency of the approach, since the reconstructed DM density profile then significantly departs from the initial one, unless one is interested in describing only the inner parts of the Galaxy (see Fig. 1 and the green curve in Fig. 5, as well as a more extended discussion on the density profile in Sec. 3.1.2). More specifically, the reconstructed density differs from the initial one by  $\sim 10\%$  above  $0.1R_{\max}$ , *i.e.*  $\sim 2r_s$ , and the difference increases even more at larger radii. Even if these numbers do not look dramatic, they still undermine the appealing aspects of this framework as a consistent and global framework for DM-signal predictions, as one loses control on the input mass model uncertainties. On the other hand, sending the boundary to infinity spoils control on the tail of the velocity distribution.

Since the speed distribution  $f_v(v, r)$  is directly related to the DF through Eq. (2.8), the divergence when  $\mathcal{E} \rightarrow 0$  translates into a divergence in velocity space when  $v^2 \rightarrow 2\psi(r)$ , *i.e.* at the escape speed and at *any* position in the system. In Fig. 2 (left panel), we illustrate this divergence in the speed distribution evaluated at a radius  $r = 20$  kpc (solid red line) in our default halo model with a radial extension set to  $R_{\max} = 500$  kpc. This divergence is the sign that the system under consideration is artificially compressed in phase space. A population of particles is squeezed near the escape speed, while we would expect a stable DF to verify  $f(\mathcal{E} \rightarrow 0) \rightarrow 0$ . The right panel of Fig. 2 shows the pathological DF  $f(\mathcal{E})$  as a function of  $\mathcal{E}$  (solid red curve), where the divergence occurs at  $\mathcal{E} \rightarrow 0$ .

This divergence is present whenever the derivative  $(d\rho/d\Psi)_{\Psi=0}$  is non-zero, which is always the case for conventional halo profiles with finite boundaries unless one modifies the asymptotic behavior at the boundaries. This issue is therefore intimately related to the

spatial extension of the system, since the troublesome derivative is evaluated at  $\Psi = 0$  (equivalently  $r = R_{\text{max}}$ ). The gravitational potential being defined up to a constant, the position  $r = R_{\text{max}}$  where  $\Psi$  vanishes is a matter of choice. For example, taking  $R_{\text{max}} \rightarrow \infty$  solves the issue and the DF satisfies  $f(\mathcal{E} \rightarrow 0) \rightarrow 0$ , as shown by the blue solid curve in the right panel of Fig. 2. This actually matches with the boundary condition of having the gravitational potential  $\psi(r) = -\phi(r) \rightarrow 0$  as  $r \rightarrow \infty$  when solving the Poisson equation. The speed distribution is then regularized—see the blue solid curve in the left panel of Fig. 2. The DF obtained for this idealized—though unrealistic—choice of  $R_{\text{max}}$  is fully consistent with the mass model and is a solution of the collisionless Boltzmann equation by construction.

This leads to the following interpretation of the divergence showing up at finite radial extensions: particles that could have probed infinite distances in agreement with the conventional infinite boundary condition are now prevented from radially escaping the system and have their phase space compressed accordingly.

However, choosing  $R_{\text{max}} \rightarrow \infty$  is physically problematic in this context. DM halos always have a finite extension due to the gravitational influence of other neighboring halos (like the dark halo of M31 in the case of our Galaxy), or the host halo if the system under consideration is a subhalo. Taking this finite extension into account is crucial for DM searches as it fixes the definition of the escape speed of the system

$$v_{\text{esc}}(r) = \sqrt{2(\phi(R_{\text{max}}) - \phi(r))}. \quad (3.1)$$

The value of the escape speed at the position of the Solar System is for instance a major ingredient when making predictions for direct WIMP searches in the low-mass region [32]. The escape speed is also a target observable that can be inferred from stellar surveys [18, 53]. Finally, in the particular case of the MW, the closest neighbor is the Andromeda galaxy which is about 800 kpc away from the Galactic center. Consequently the Galactic halo cannot extend much farther than  $R_{\text{max}} \sim 500$  kpc, which we take as our reference value from now on.<sup>2</sup>

In the left panel of Fig. 3, we compute the relative change in the escape speed when increasing the value of  $R_{\text{max}}$ . One can see that the escape speed at  $r = 8$  kpc increases by up to 10% ( $\sim 50$  km/s) when the radial boundary moves further out. The relative increase gets bigger as the position is farther away from the center of the halo, though lower in absolute value. It is therefore important to be as consistent as possible when one wants to relate the concept of escape to the phase-space DF.

The discussion above focused on the isotropic case, but the situation is very similar in the anisotropic case with a constant anisotropy parameter  $\beta$ . Sending  $R_{\text{max}}$  to infinity removes the diverging term in  $G(\mathcal{E})$  [see Eq. (2.16)], and the DF is regularized at the cost of changing the escape speed. However, the situation is different in the Osipkov-Merritt case, as the troublesome derivative is  $(d\rho_{\text{OM}}/d\Psi)_{\Psi=0}$  with  $\rho_{\text{OM}}$  defined in Eq. (2.26). One can check that if the density behaves as a power-law at large radii  $\rho \propto r^{-b}$ —as is almost always the case—then  $d\rho_{\text{OM}}/dr \propto r^{1-b}$  and  $d\Psi/dr \propto r^{1-b}$ , meaning that the derivative  $(d\rho_{\text{OM}}/d\Psi)_{\Psi=0}$  goes to a constant as  $R_{\text{max}}$  goes to infinity. Consequently, in the Osipkov-Merritt model, not only does considering an infinite system affect the escape speed, but it also does not remove the phase-space divergence, as illustrated in the right panel of Fig. 3. Moreover, for this model the divergence in the speed distribution (Eq. 2.8) does not occur at  $v_{\text{esc}}$  but appears in the peak of the distribution due to the angular integral. This makes it more difficult to regularize the DF.

<sup>2</sup>Note that  $R_{\text{max}}$  is almost twice as large as the estimated virial radius  $R_{200} \sim 250$  kpc.

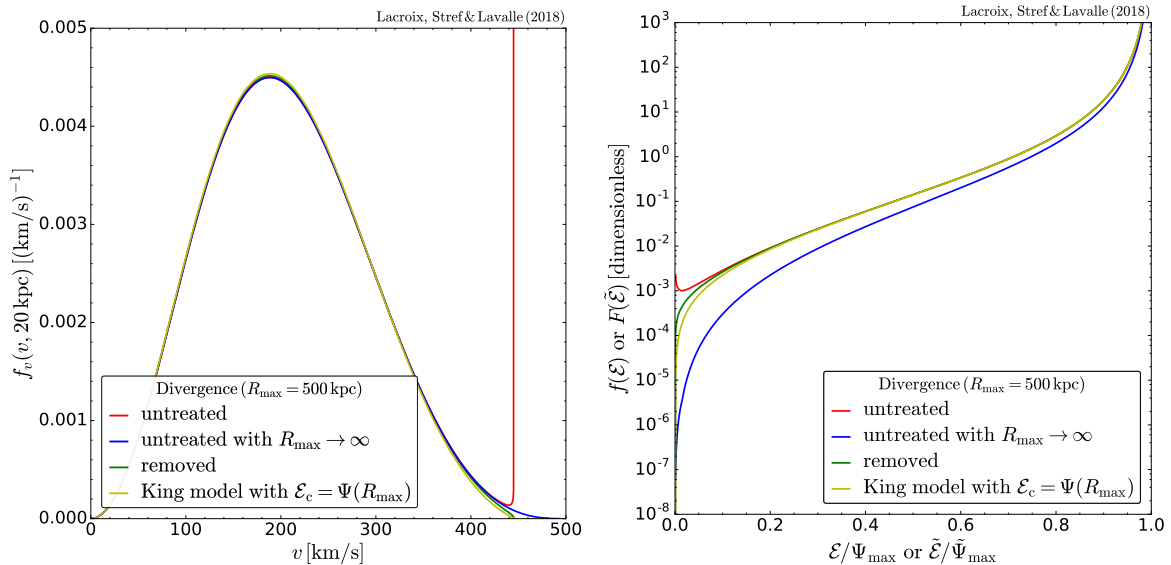


**Figure 2:** **Left panel:** Velocity distribution functions (i) for the NFW profile of Ref. [39] at a radius of 20 kpc, for three situations regarding the status of the divergence at the escape velocity; and (ii) for the regularization à la King given in Eq. (3.11). The red, blue, green, and yellow lines represent the DFs obtained by keeping the divergence, sending the boundary of the system to infinity, removing the divergence, and using the regularization à la King, respectively. **Right panel:** Corresponding DFs as a function of the energy  $\mathcal{E}$ . DFs are in units of  $\rho_s (4 \pi G_N \rho_s r_s^2)^{-3/2}$ .

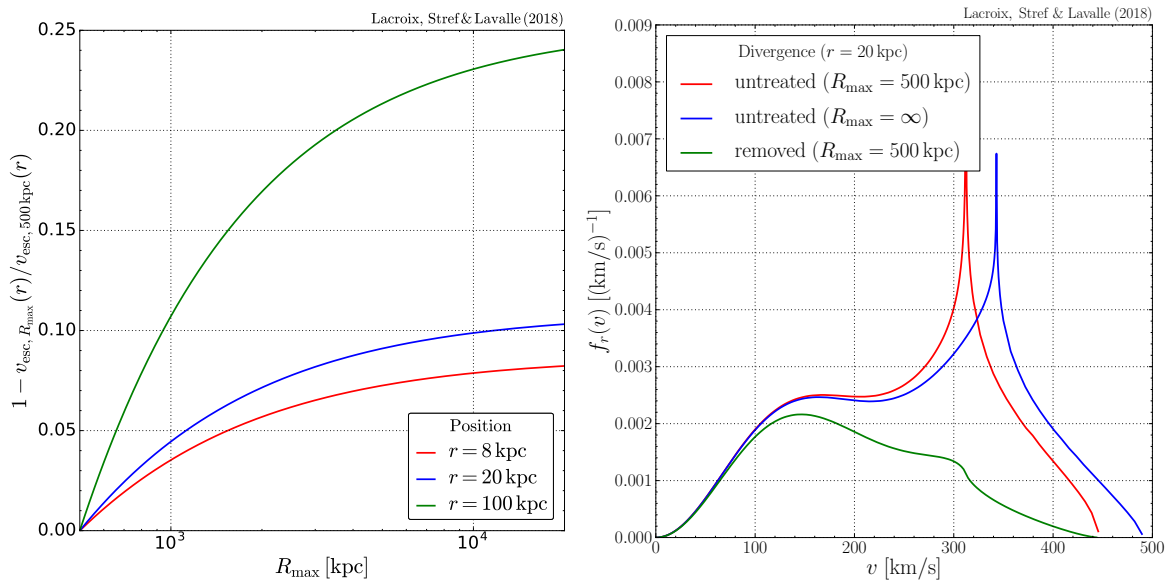


**Figure 3:** **Left panel:** Relative variation of the escape velocity at a position  $r$  as the system's boundary  $R_{\text{max}}$  is modified (the reference value is set to  $R_{\text{max}} = 500 \text{ kpc}$ ). **Right panel:** Same as left panel of Fig. 2, for the Osipkov-Merritt model.

In the following, we discuss different ways of getting rid of this divergence in order to obtain physically viable solutions.

### 3.1.2 Regularization through the density profile

The most simple solution to the boundary-induced divergence is to slightly modify the DM density profile in such a way that it is still consistent with the kinematic constraints which it was derived from, and that  $(d\rho/dr)_{r=R_{\max}}$  vanishes—this is not the case with standard NFW,  $\alpha\beta\gamma$ , or Einasto profiles. If such a solution exists, then the Eddington formalism fully applies and provides a self-consistent description of the phase space up to the spatial boundary of the DM halo. Therefore, since the bulk of the kinematic constraints pertains to the inner 50 kpc of the Galaxy [39], we need to make sure that both the input DM mass profile and gravitational potential are not affected in this range. The kinematics of satellite galaxies can also be used to constrain the MW mass within  $\sim 300$  kpc with larger uncertainties (see *e.g.* Ref. [54]), but not farther, so the modified mass profile should not depart too much from the initial one and remain consistent with these bounds.

Modifications of standard functional forms of the density profile can be found in the literature. For instance, the authors of Ref. [55] (see also Ref. [56]) account for tidal stripping of the outer parts of a halo with an exponential suppression. However, this modified profile has  $(d\rho/d\Psi)_{\Psi=0} \neq 0$  and therefore leads to a diverging DF once we set a radial boundary. Instead, we propose the following alternative density profile to model the halo:

$$\tilde{\rho} = \rho - \Psi_{\text{D}} \left( \frac{d\rho}{d\Psi_{\text{D}}} \right)_{\Psi=0}. \quad (3.2)$$

The corresponding DM component, the gravitational potential of which is  $\Psi_{\text{D}}$ , is consistently obtained from the Poisson equation (with the vanishing condition at the radial boundary  $R_{\max}$ ), which then reduces to

$$\begin{aligned} \tilde{\Psi}_{\text{D}}(r) &= G \int_r^{R_{\max}} dr' \frac{\tilde{m}_{\text{D}}(r')}{r'^2} \\ \text{where } \tilde{m}_{\text{D}}(r) &= 4\pi \int_0^r dr' r'^2 \tilde{\rho}(r'). \end{aligned} \quad (3.3)$$

This potential is the one to be used in the Eddington inversion along with the modified density profile  $\tilde{\rho}$  (the baryonic component is left unchanged). That new density profile  $\tilde{\rho}$ , defined in Eq. (3.2), flattens at the edge of the system, *i.e.*

$$(d\tilde{\rho}/d\tilde{\Psi})_{\tilde{\Psi}=0} = [(d\tilde{\rho}/dr)(d\tilde{\Psi}/dr)^{-1}]_{r=R_{\max}} = 0.$$

This flattening at  $r \rightarrow R_{\max}$  can be thought of as the border with the homogeneous background or with neighboring self-gravitating systems (though physical space cannot be filled up with spheres). This functional form is actually guided by the reconstructed density profile obtained when removing the divergence by hand, as discussed in Sec. 3.1.3.

This prescription needs slight modifications when dealing with anisotropic systems since the diverging term takes a different form in that case. In the constant- $\beta$  case this term is proportional to  $(d\chi/d\Psi)_{\Psi=0}$  where  $\chi = r^{2\beta_0}\rho$ , therefore we propose the following profile:

$$\tilde{\rho} = \rho - \frac{\Psi_{\text{D}}}{r^{2\beta_0}} \left( \frac{d^n \chi}{d\Psi_{\text{D}}^n} \right)_{\Psi_{\text{D}}=0}, \quad (3.4)$$

where  $\chi$  is defined in Eq. (2.17) and  $n$  is given in Eq. (2.21). For the Osipkov-Merritt models

$$\tilde{\rho} = \rho - \frac{\Psi_{\text{D}}}{1 + r^2/r_{\text{a}}^2} \left( \frac{d\rho_{\text{OM}}}{d\Psi_{\text{D}}} \right)_{\Psi_{\text{D}}=0}. \quad (3.5)$$

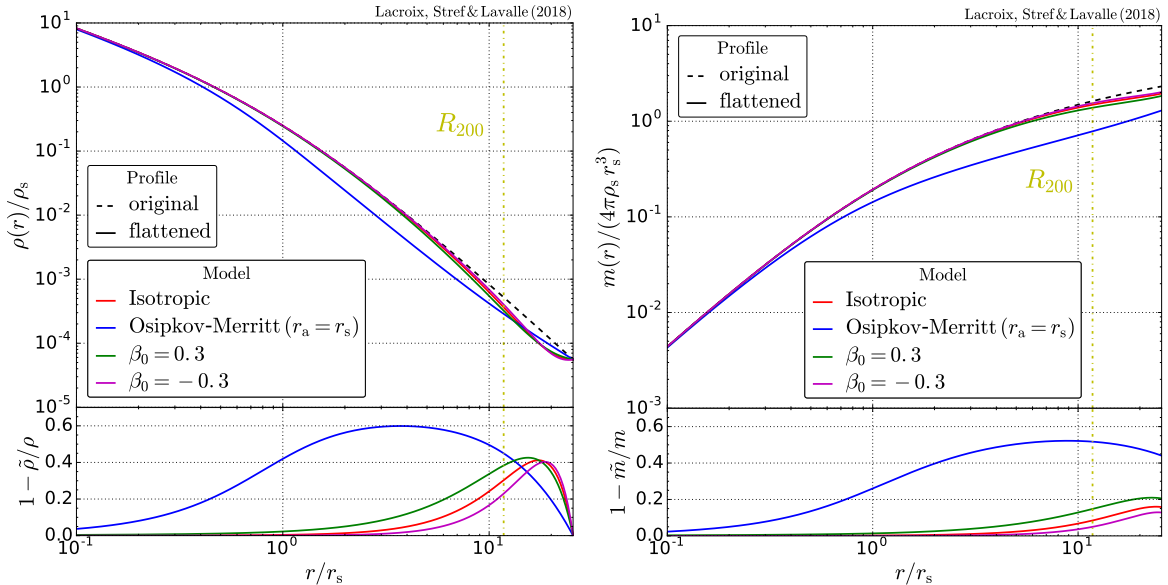


**Figure 4:** **Left panel:** Density profile  $\rho$  in the standard NFW case (black line) compared to the modified profiles for the isotropic, Osipkov-Merritt,  $\beta = \pm 0.3$  (red, blue, green and magenta, respectively) defined in Eqs. (3.2), (3.4), (3.5). The bottom panel shows the relative difference between the original and the modified profile. **Right panel:** Same as for left panel, for the mass profile.

In these two cases, the gravitational potential is consistently calculated from Eq. (3.3). Note that in the anisotropic case, the modified profile depends on the anisotropy variable ( $\beta_0$  or  $r_a$ ) specific to the model.

The modified density and mass are compared to the original ones in Fig. 4. The modified density differs from the original one in the outer part of the halo, and underestimates the original profile by up to 40% at  $\sim 0.8 R_{\max}$  (30% at  $R_{200}$ ) in the isotropic case, which translates into a difference in the mass of only 15% at  $r = R_{\max}$  (10% at  $R_{200}$ ). The inner, dynamically constrained part of the profile is therefore kept mostly unchanged by the prescription when the system is isotropic. The introduction of a constant anisotropy causes a departure from the isotropic result in a systematic way that depends on the sign of  $\beta_0$ . The difference in density and mass is higher in the  $\beta_0 > 0$  case than in the isotropic and  $\beta_0 < 0$  cases, which is consistent with the expectation for more radial orbits. The difference for Osipkov-Merritt models is even bigger: the mass difference reaches 50% at  $R_{200}$ . These differences can be understood in terms of the anisotropy of the system. Our prescription removes matter at the edge of the halo to flatten the density profile at  $R_{\max}$ . However, if the particles at  $R_{\max}$  are mostly on radial orbits, as is the case in the Osipkov-Merritt models where  $\beta(R_{\max}) \simeq 1$ , they also contribute to the density in the inner part of the halo. Therefore in a system with a high positive  $\beta$ , removing matter in the outskirts also removes matter in the inner regions.

To summarize, we found that slight modifications of the density profile are enough to get rid of the boundary-induced divergence in the isotropic case and in the case of tangential anisotropy, while keeping the overall mass model consistent with the constrained initial configuration. Indeed, the error induced on the Galactic mass at large radii is of order  $\sim 10\%$  in these cases. Therefore, such modifications preserve the self-consistency of the formalism, and do not affect the density- and velocity-dependent observables related to DM



searches calculated in the inner  $\sim 50$ -100 kpc of the MW. Errors of  $\gtrsim 10\%$  are expected in the outskirts, but should be negligible *e.g.* when integrated over the line of sight, like in the case of  $p$ -wave suppressed or Sommerfeld-enhanced annihilation calculations. On the other hand, this regularization procedure fails in the case of significant radial anisotropy, like in the Osipkov-Merritt model, unless the anisotropy radius is taken very large (isotropy limit).

### 3.1.3 Regularization through the phase-space distribution

The problem of the spatial boundaries in self-gravitating systems is rather classical when one takes the DF as the fundamental characterizing function. A well-known example is the so-called King model [17, 57–61], meant to consistently describe bounded pseudo-isothermal systems (and applied to globular clusters). For the boundary-induced divergence at stake in our study, one can apply a similar procedure by (i) cutting the non-physical diverging term in the phase-space DF  $f(\mathcal{E})$ ; (ii) numerically deriving the modified gravitational potential from the Poisson equation fed by the new DF and appropriate boundary conditions (this is an important step which also defines the new mapping between the potential and the radial coordinate); and (iii) integrating the new DF to get the modified density profile. Although much more involved than the regularization through the density presented in Sec. 3.1.2, this method ensures to get a well-behaved solution consistent with both the Boltzmann equation and the Poisson equation. It is particularly well-suited to describe bounded systems like galaxies [62], and also to account for tidal effects induced by either neighboring systems like dwarf galaxies [36, 63, 64], or hosted systems, like DM subhalos [65, 66]. In the present context, one still needs then to make sure that the modified density profile does not depart too much from the initial density profile, at least within the inner 50-100 kpc of the MW, not to spoil its consistency with kinematic data.

Before inspecting possible ways of cutting the initial DF  $f(\mathcal{E})$ , let us review the full chain of calculations. Let us call  $F(\tilde{\mathcal{E}})$  the modified DF after truncation, where

$$\tilde{\mathcal{E}} = \tilde{\Psi} - \frac{\tilde{v}^2}{2} \quad (3.6)$$

is the new energy associated with the system,  $\tilde{\Psi}$  the new potential, and  $\tilde{v}$  the new velocity coordinate. A priori, tilde quantities are different from non-tilde quantities that pertain to the initial configuration. However, since  $F(\tilde{\mathcal{E}})$  is known (inferred from a modification of  $f(\mathcal{E})$  that we shall discuss later), we can fully determine the DM component of the gravitational potential from the Poisson equation

$$\begin{aligned} \Delta \tilde{\Psi}_D &= -4\pi G_N \tilde{\rho}(\tilde{\Psi}) = -4\pi G_N \int d^3\tilde{v} F(\tilde{\mathcal{E}}) \\ &= -4\pi G_N \left[ \tilde{\rho}_0 + 4\pi\sqrt{2} \int_0^{\tilde{\Psi}} \sqrt{\tilde{\Psi} - \mathcal{E}} F(\mathcal{E}) d\mathcal{E} \right], \end{aligned} \quad (3.7)$$

where though the density profile  $\tilde{\rho}$  is still undetermined, it is accessed through the integral of the DF over the potential. Note that  $\tilde{\Psi} = \tilde{\Psi}_D + \tilde{\Psi}_B$ , and that only the DM component is modified, such that we actually take  $\tilde{\Psi}_B = \Psi_B$ . An important point here is that the mapping between the radial coordinate and  $\tilde{\Psi}$  is only defined through the Laplacian operator  $\Delta$  on the left-hand side, not on the right-hand side. Therefore, one needs appropriate boundary conditions to solve this equation consistently with the physical system at hand. In the present context, we are in principle forced to demand that  $\tilde{\Psi}(R_{\max}) = 0$ , and since we do

not want a significant departure from the initial potential in the inner parts of the Galaxy, we further impose that  $d\tilde{\Psi}/dr(0) = d\Psi/dr(0)$ . Besides, note that we allow for the presence of a constant  $\tilde{\rho}_0$  in the above equation, which is a free parameter and cannot be recovered from the equation itself. This freedom in choosing the value of the density at the boundary of the system is inherent to the Eddington formalism as previously seen in Eq. (2.14)—note that it can be neglected here as the density profile is no longer an input in the regularization procedure, but an output. Finally, we stress that the above differential equation has to be solved numerically.

We now discuss some possible forms for the modified DF  $F$ , which are to be considered as ansätze aimed at recovering the non-diverging part of the initial DF while ensuring that  $F(\tilde{\mathcal{E}} \rightarrow 0) \rightarrow 0$ . We first consider the Eddington DF computed for a finite system with radial extension  $R_{\max}$ . The initial DF is given in Eq. (2.13) and diverges as  $\mathcal{E} \rightarrow 0$ . One way of modifying that DF to get a well-behaved distribution is simply to remove the diverging term  $\propto 1/\sqrt{\mathcal{E}}$ . The modified DF is then

$$F(\tilde{\mathcal{E}}) = f(\tilde{\mathcal{E}}) - \frac{1}{\sqrt{8\pi^2}} \frac{1}{\sqrt{\tilde{\mathcal{E}}}} \left( \frac{d\rho}{d\Psi} \right)_{\Psi=0} = \frac{1}{\sqrt{8\pi^2}} \int_0^{\tilde{\mathcal{E}}} \frac{d^2\rho}{d\Psi^2} \frac{d\Psi}{\sqrt{\tilde{\mathcal{E}} - \Psi}}. \quad (3.8)$$

Such an ansatz makes sense only if  $\tilde{\mathcal{E}}$  spans the same range as  $\mathcal{E}$  (note that  $\rho$  and  $\Psi$  are non-tilde quantities). This is possible only if the condition  $\tilde{\Psi}_{\max} = \tilde{\Psi}(r=0) = \Psi(r=0)$  is obeyed, which is in contradiction with the presumed boundary condition to solve Eq. (3.7), *i.e.*  $\tilde{\Psi}(R_{\max}) = 0$ . The latter condition must therefore be traded for the former in that case, and the spatial boundary of the system is no longer  $R_{\max}$ , but a new  $\tilde{R}_{\max}$ . In practice, though, we find that  $\tilde{R}_{\max} \approx R_{\max}$ , such that the above ansatz can still be applied.

Since in the initial DF the diverging term becomes important only as  $\mathcal{E} \rightarrow 0$ , we expect the modified potential to remain close to the original one which allows us to estimate the modified density from the Abel equation

$$\frac{d\tilde{\rho}}{d\tilde{\Psi}} = \sqrt{8\pi} \int_0^{\tilde{\Psi}} \frac{F(\mathcal{E})}{\sqrt{\tilde{\Psi} - \mathcal{E}}} d\mathcal{E}. \quad (3.9)$$

Assuming  $\tilde{\Psi} \approx \Psi$  and  $\tilde{\rho}(\tilde{\Psi} = 0) \approx \rho(\Psi = 0)$ , we get

$$\tilde{\rho} \approx \rho - \Psi \left( \frac{d\rho}{d\Psi} \right)_{\Psi=0}. \quad (3.10)$$

The modification of the constant- $\beta$  DF is very similar, except the modification is only performed on the energy-dependent part of the DF  $G(\mathcal{E})$  in Eq. (2.16). The modification of the Osipkov-Merritt models is identical to the isotropic case with the change  $\mathcal{E} \rightarrow Q$ . However, Fig. 3 shows that removing the divergence by hand leads to a huge modification of the speed distribution. As a result, the Osipkov-Merritt DF is very hard to regularize in a self-consistent way.

Note that the above expression for  $\tilde{\rho}$  is similar to the one proposed in Eq. (3.2), except that the potential that appears is the DM only potential rather than the total potential. The density and mass shown in Fig. 4 are therefore also relevant for the modified DF discussed here.

We now turn to a truncation of the DF more fundamentally inspired from the King model [17]. The original approach focused on making isothermal spheres finite in phase

space but was later generalized to generic mass distributions (see *e.g.* [62]). It was also very recently used to implement a realistic tidal truncation of satellite DM halos [63]. The spirit of the method is slightly different from what was presented just above in the sense that we no longer start from a diverging and ill-defined DF, but from a well-behaved DF describing a self-gravitating system with spatial boundaries sent to infinity (thereby resembling the King model, which starts from the Maxwellian DF that describes the infinite isothermal sphere). In the isotropic case, this initial DF is precisely the Eddington function  $f(\mathcal{E})$  given in Eq. (2.13), taking the gravitational potential  $\Psi(r) = -\phi(r)$  as the solution to Poisson’s equation with the boundary condition  $\phi(r \rightarrow \infty) \rightarrow 0$ . We then implement a truncation in energy related to the desired radial boundary  $R_{\max}$  from a procedure similar to the one introduced above: (i) cut the phase-space volume in energy below a cutoff  $\mathcal{E}_c = \Psi_0 = \Psi(R_{\max})$ ; (ii) define a new phase-space DF  $F(\tilde{\mathcal{E}} \equiv \mathcal{E} - \Psi_0)$  from  $f(\mathcal{E})$  above the cutoff, with the expected asymptotic behavior  $F(\tilde{\mathcal{E}} \rightarrow 0) \rightarrow 0$ ; (iii) determine the new associated gravitational potential  $\tilde{\Psi}$  from Eq. (3.7) (as previously, this defines the new mapping between the radial coordinate and the potential); (iv) integrate the new DF to get the modified density profile  $\tilde{\rho}$ .

According to this procedure, the ansatz for the modified DF  $F$  that relates a cutoff in energy to a radial cutoff is then defined as

$$F(\tilde{\mathcal{E}}) = \begin{cases} f(\tilde{\mathcal{E}} + \Psi_0) - f(\Psi_0) & \text{for } \tilde{\mathcal{E}} \geq 0 \\ 0 & \text{for } \tilde{\mathcal{E}} < 0 \end{cases} \quad (3.11)$$

This DF is continuous and satisfies  $F(\tilde{\mathcal{E}} = 0) = 0$  by construction. The associated gravitational potential  $\tilde{\Psi}$  is solution of the Poisson equation Eq. (3.7), with initial conditions to be specified. If we set the cutoff in the initial DF to  $\mathcal{E}_c = \Psi_0 = \Psi(R_{\max})$ , then  $\tilde{\Psi}_{\max} = \Psi_{\max} - \Psi(R_{\max})$  by construction, which by no means guarantees that  $\tilde{\Psi}$  vanishes at  $R_{\max}$ . In practice though, we find that the radius  $\tilde{R}_{\max}$  at which  $\tilde{\Psi}(\tilde{R}_{\max}) = 0$  is very close to  $R_{\max}$ , though slightly larger. To get  $\tilde{\Psi}(R_{\max}) = 0$  directly from the Poisson equation, one would instead need to tune the initial cutoff potential  $\Psi_0$  until equality is reached—in the same vein, we find in that case that  $\Psi_0 \approx \Psi(R_{\max})$ .

Note that unlike removing the diverging term “by hand”, the King approach may lead to a physical interpretation in terms of tidal cut, since it has been shown in numerical simulations that tidal stripping tends to remove particles based on their energy rather than their angular momentum [67]. In the present context, such stripping could have resulted from gravitational interactions with the neighboring galaxies. We show the dark halo profile reconstructed from the DF of Eq. (3.11) after solving Eq. (3.7) in Fig. 5, where the difference in setting the cutoff discussed just above is illustrated explicitly.

### 3.1.4 Regularization of the boundary-induced divergence: Summary

Here we summarize the pros and cons of the regularization procedures implemented above to remove the radial boundary-induced divergence of the phase-space DF as  $\mathcal{E} \rightarrow 0$  or equivalently  $v \rightarrow v_{\text{esc}}$ . For the isotropic case, we saw that the technically easiest way to remove the divergence while ensuring the self-consistency of the Eddington inversion method was to slightly modify the input density profile around the radial boundary  $R_{\max}$  in such a way that the dynamics is unaffected in the central regions of the Galaxy. In that case, one can straightforwardly find the new gravitational potential  $\tilde{\Psi}_D$  by directly integrating the Poisson equation over the radial coordinate from Eq. (2.4). The regularization through modifications of the DF is more involved as it requires to calculate  $\tilde{\Psi}_D$  by numerically solving the Poisson equation. This is the only way to recover a mapping between the potential and the radial

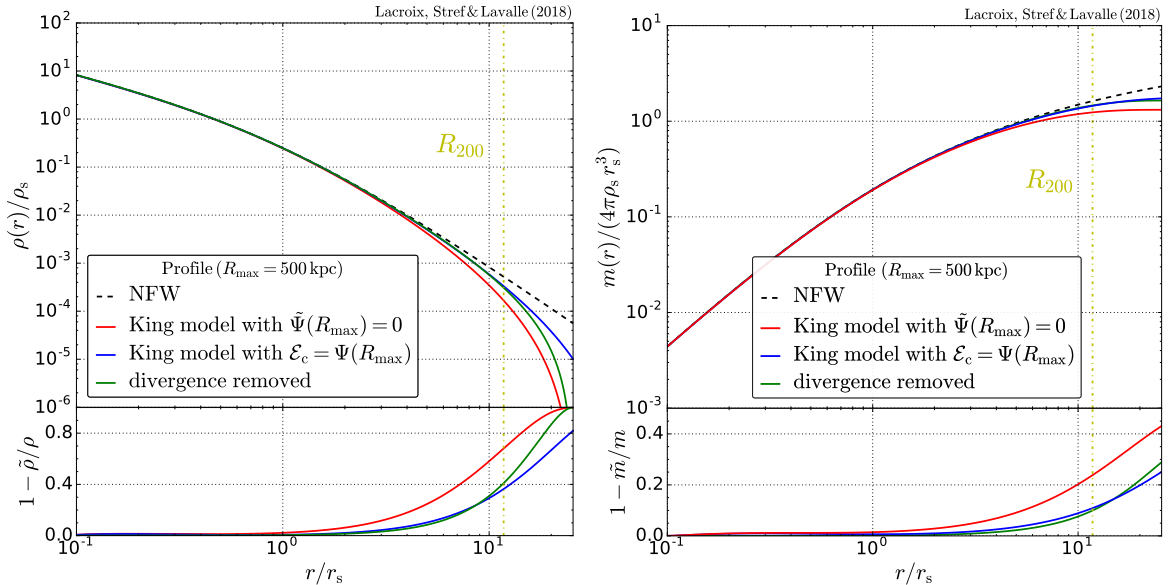


**Figure 5:** Same as Fig. 4, showing the profiles resulting from DFs regularized à la King, based on the ansatz of Eq. (3.11). **Left panel:** reconstructed density profiles compared with the initial one. **Right panel:** corresponding dark halo mass profiles.

coordinate, and then to compute the resulting modified density profile. Both methods give similar distortions to the initial density profile, which lie within the current statistical and systematic uncertainties on the dark halo mass profile. Ultimately, the best, while much more involved approach, would be to start from well-defined DF and profile before performing the likelihood analysis to account for the kinematic constraints and to get best-fitting Galactic mass models, similar to the action-angle analyses (*e.g.* [50]). This goes beyond the scope of this paper.

For anisotropic systems, we saw that both methods may apply to tangential anisotropy ( $\beta < 0$ ), but fail for radial anisotropy (both  $\beta > 0$  and the Osipkov-Merritt models). In the latter case, the only way to get finite results is to remove the diverging term ( $\propto 1/\sqrt{\mathcal{E}}$  or  $\propto 1/\sqrt{Q}$ ) by hand, but this is at the cost of a meaningful and self-consistent normalization of the phase-space DF. Therefore, we are then left with a theory that is no longer a self-consistent inversion of the integral Eq. (2.7), whose DF must be normalized to unity (or  $\rho$  or  $\tilde{\rho}$ ) by hand and is no longer simply related to the DM density profile. Although such a DF might be perfectly licit as a description of a gravitational system, its theoretical status appears unclear to us.

### 3.2 Positivity and stability issues

We now move to another kind of issues that may arise in the Eddington formalism: the potential breakdown of the inversion, very often due to the presence of baryonic components. More concretely, it turns out that some perfectly sound configurations of Galactic mass models may lead to ill-defined DFs through this method, which are the manifestation of unstable configurations in phase space. In these cases, Eddington-like inversions can no longer be used to self-consistently describe the DM halo, because some degrees of freedom are likely missing to make full physical sense of the DM component (axisymmetry, action-angles coordinates, *etc.*). We stress that the potential breakdown of the Eddington formalism

may only manifest itself in some regions of the phase space. This is actually barely checked in the context of predictions for direct DM searches. A typical signature of such a breakdown is a DF exhibiting negative values in specific regions of phase space, which will be discussed in Sec. 3.2.1. More subtle while complementary considerations linked to the stability of gravitational systems will be discussed in Sec. 3.2.

### 3.2.1 Positive distribution functions

A trivial requirement for a DF to be well-behaved is positivity everywhere, *i.e.*  $f(\vec{r}, \vec{v}) \geq 0$  for any  $(\vec{r}, \vec{v})$ . Although most dark halo shapes are fully Eddington invertible for DM-only systems (*e.g.* [68]), there is in general no guarantee that Eddington's inversion leads to a DF positive all over the halo for any given pair of DM density profile  $\rho$  and total gravitational potential  $\Psi = \Psi_D + \Psi_B$ . We will inspect below the specific case of cored profiles, but it usually turns out that the presence of a baryonic component, which breaks the plain correlation between the density and the potential, may drive the DF negative in some regions of the system.

Sufficient conditions for positivity were identified in Refs. [69, 70] for the Osipkov-Merritt models, in the general case of multi-component systems. From Eq. (2.29) we can identify a necessary condition for the positivity of  $f_{OM}$ , which is

$$\frac{d\rho_{OM}}{d\Psi} \geq 0 \text{ for } 0 \leq \Psi \leq \Psi_{\max}. \quad (3.12)$$

In this equation,  $\rho_{OM}$  corresponds to the DM while  $\Psi = \Psi_D + \Psi_B$  is the total potential (from the DM plus baryons). If this necessary condition is satisfied, a sufficient condition for positivity is [69, 70]

$$\frac{d}{d\Psi_D} \left[ \frac{d\rho_{OM}}{d\Psi_D} \left( \frac{d\Psi}{d\Psi_D} \right)^{-1} \sqrt{\Psi} \right] \geq 0 \quad \forall 0 \leq \Psi \leq \Psi_{\max}. \quad (3.13)$$

One can readily see that these conditions are also valid for isotropic systems as well as single component systems. All McM17 halo profiles verify this condition.

Let us return to the isotropic case and inspect it in detail. Most standard single-component mass distributions (*e.g.* NFW, Einasto, *etc.*) have well-defined ergodic DFs [68]. Yet, some well-motivated profiles do lead to a negative DF. Troublesome profiles can be identified using Eq. (2.11). If the derivative  $d\rho/d\Psi_D$  cancels for some values of  $\Psi_D$ , then Eq. (2.11) forces  $f$  to take negative values. This is expected to happen if the DM profile is very flat somewhere, as is the case for cored distributions for instance. In the case of single-component systems, the left-hand side of Eq. (2.11) can be written

$$\frac{d\rho}{d\Psi_D} = \frac{dr}{d\Psi_D} \frac{d\rho}{dr} = -\frac{r^2}{G m_D(r)} \frac{d\rho}{dr}, \quad (3.14)$$

where the mass  $m_D(r)$  is related to the density  $\rho(r)$  through Eq. (2.5). Let us now consider as an example the following class of cored DM density profiles:

$$\rho(r) = \rho_s \left[ 1 + \left( \frac{r}{r_s} \right)^\alpha \right]^{-\beta/\alpha}, \quad (3.15)$$

with  $\alpha > 0$  and  $\beta > 0$ . In the limit  $r \rightarrow 0$  (equivalently  $\Psi_D \rightarrow \Psi_{\max}$ ) we have  $d\rho/dr \propto r^{\alpha-1}$  and  $m \propto r^3$ , therefore  $d\rho/d\Psi_D \propto r^{\alpha-2}$ . The asymptotic value of the derivative is then non-zero only if  $\alpha \leq 2$ . Consequently, for *any* single-component system with a density profile

given by Eq. (3.15) and with  $\alpha > 2$ , the Eddington method leads to a negative ergodic DF. We stress that

$$0 < \alpha \leq 2 \text{ is a } \textit{necessary} \text{ condition (isotropic case)} \quad (3.16)$$

to get a positive DF for a DM-only system. However, it is certainly not sufficient for a multi-component system. Since the argument is based on the asymptotic behavior of  $d\rho/d\Psi_D$  as  $r \rightarrow 0$ , our result holds for Osipkov-Merritt models as well since the associated anisotropy goes to zero when  $r \ll r_a$ . In the constant anisotropy case the situation is different because an artificial slope  $2\beta_0$  is present in the Abel equation given in Eq. (2.19). Consequently, if the density profile  $\rho$  has an inner slope  $-\gamma$ , the pseudo-density  $\chi$  has an inner slope  $2\beta_0 - \gamma$ . Note that a requirement for Eddington's method and its extensions to work is that the generalized density ( $\rho$ ,  $\rho_{OM}$ ,  $\chi$  depending on the model) is a growing function of  $\Psi$ . Therefore,

$$2\beta_0 \leq \gamma \text{ is a } \textit{necessary} \text{ condition (anisotropic } \beta_0 \text{ case)} \quad (3.17)$$

to get a positive constant-anisotropy DF. This forbids for instance any cored system to have a constant, positive anisotropy, and in general sets an upper limit on the constant anisotropy a system can feature. This is a subset of a more general slope-anisotropy inequality [71, 72].

Adding a baryonic component to the system can affect these results. If the DM profile follows Eq. (3.15) and the baryonic profile is cored, the low-radius behavior of  $d\rho/d\Psi$  (with  $\Psi = \Psi_D + \Psi_B$  the total potential) is unchanged with respect to that of  $d\rho/d\Psi_D$ . Therefore, the positivity condition remains  $\alpha \leq 2$ . If the baryonic density profile is cuspy with inner slope  $-\gamma_B$  (e.g.  $\gamma_B = 1$  for a Hernquist profile), the result is modified. The mass is now dominated by the baryonic component as  $r \rightarrow 0$ , and we have  $d\rho/d\Psi \propto r^{\alpha-2+\gamma_B}$ . The necessary condition for positivity becomes

$$0 < \alpha \leq 2 - \gamma_B \quad (3.18)$$

*i.e.* baryons reduce the parameter space providing a positive DF.

### 3.2.2 Stable distribution functions

We would like to stress here that positivity is not strong enough a criterion for a DF to give a satisfactory description of a DM halo. Indeed, some  $(\rho, \Psi)$  pairs satisfying the positivity conditions can still lead to a DF that is an *unstable* solution of the collisionless Boltzmann equation. Some conditions for stability against different kinds of perturbations are reviewed in Ref. [40]. A result of interest for us is Antonov's second law [73–75] which guarantees the stability of an ergodic DF  $f$  against non-radial modes if  $df/d\mathcal{E} > 0$ . A complementary result is the Doremus-Feix-Baumann theorem [76, 77], which ensures stability against radial modes if  $df/d\mathcal{E} > 0$ . Consequently, a *sufficient condition for the stability* of ergodic DFs  $f(\mathcal{E})$  against all perturbations is

$$\frac{df}{d\mathcal{E}}(\mathcal{E}) > 0 \text{ for all } \mathcal{E}. \quad (3.19)$$

We now investigate the consequences of this condition on DM density profiles. In practice we use profiles of the form of Eq. (3.2) in order to get rid of the divergence discussed in Sec. 3.1. Note that we previously established that this divergence is a sign of an artificial compression of the phase space, but it can also be viewed as an unstable configuration as it violates the

stability criterion given in Eq. (3.19). We wish to find a more convenient criterion involving the density profile and the potential rather than the DF itself. We recall the expression of the DF when the boundary term is zero:

$$f(\mathcal{E}) = \int_0^{\mathcal{E}} \frac{d^2\rho}{d\Psi^2} \frac{1}{\sqrt{\mathcal{E} - \Psi}} d\Psi. \quad (3.20)$$

From this expression we see that  $df/d\mathcal{E} > 0, \forall \mathcal{E}$  only if  $d^2\rho/d\Psi^2 > 0, \forall \Psi$ . Moreover, starting from the Abel equation in Eq. (2.11) and performing an integration by parts, we get

$$\frac{d\rho}{d\Psi} = 2\sqrt{8\pi} \int_0^{\Psi} \sqrt{\Psi - \mathcal{E}} \frac{df}{d\mathcal{E}} d\mathcal{E}, \quad (3.21)$$

which implies that  $d^2\rho/d\Psi^2 > 0, \forall \Psi$  only if  $df/d\mathcal{E} > 0, \forall \mathcal{E}$ . To summarize, we have

$$\frac{df}{d\mathcal{E}} > 0, \forall \mathcal{E} \iff \frac{d^2\rho}{d\Psi^2} > 0, \forall \Psi. \quad (3.22)$$

Therefore, the stability criterion takes the very simple following form:  $d^2\rho/d\Psi^2 > 0, \forall \Psi$ . From Eq. (3.20), it is obvious that this criterion is also a sufficient condition for positivity. From now on, we consider Eq. (3.22) as defining the range of applicability of the Eddington formalism since a system that violates this condition could lead to unstable phase-space configurations or a negative DF.

The stability criterion of Eq. (3.22) can be extended in part to non-isotropic spherical systems with a DF of the form  $f(\mathcal{E}, L)$ . It is shown in Ref. [78] that systems satisfying  $\partial f/\partial \mathcal{E} > 0$  for all  $(\mathcal{E}, L)$  are stable against radial perturbations. This is directly applicable to the constant- $\beta$  (Eq. 2.16) and Osipkov-Merritt (Eq. 2.24) models, resulting in

$$\frac{dG}{d\mathcal{E}} > 0, \forall \mathcal{E} \quad (3.23a)$$

$$\frac{df_{\text{OM}}}{dQ} > 0, \forall Q. \quad (3.23b)$$

However, the response of anisotropic systems to non-radial perturbations is much more complex, due to the possibility of radial-orbit instabilities, so that no simple stability criteria are known. Analytical studies are usually involved (*e.g.* [79–82]), and the stability properties of anisotropic systems are very often investigated thanks to numerical simulations (*e.g.* [83–85]), which is far beyond the scope of this work. In the following, we rely on the criterion given in Eq. (3.23), which should be understood as necessary rather than sufficient.

We investigated the stability of the phase-space configurations obtained by Eddington-inverting realistic and kinematically constrained McM17 MW dark halos [39]. Shown in the top left panel of Fig. 6 are the isotropic DFs for each mass model, both with and without the baryonic contribution to the potential  $\Psi$ . To simplify the discussion, the DFs are shown *without* the diverging term discussed in Sec. 3.1, and without any regularization plugged in. Indeed, we will see that in these examples, instabilities manifest themselves mostly in the central regions of the Galaxy, *i.e.*  $\mathcal{E}/\Psi_{\text{max}} \gtrsim 0.5$ . The dark halos shown in the figure mostly differ in the inner slope  $\gamma$  of the density profile. In the absence of baryons (dashed lines), all the DFs satisfy the stability criterion given in Eq. (3.19) and are therefore stable. We explicitly verified that the models also satisfy the condition in Eq. (3.22) by plotting the second-order derivative  $d^2\rho/d\Psi^2$  in the top right panel of Fig. 6.

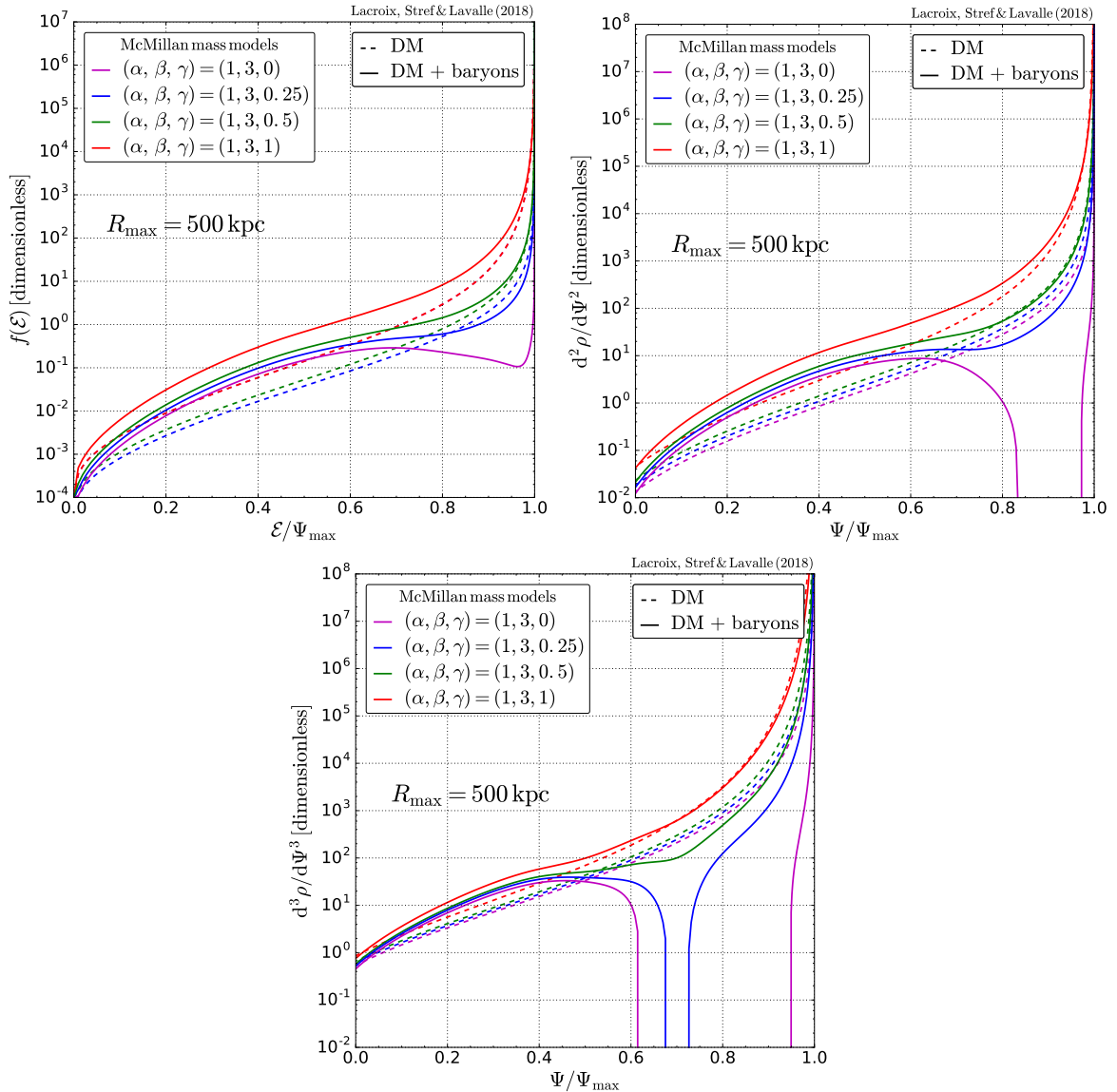


**Figure 6:** **Top left panel:** Ergodic distribution functions for several mass models from Ref. [39]. The DFs are in units of  $(4\pi G_N)^{-3/2} \rho_s^{-1/2} r_s^{-3}$ . **Top right panel:** Second derivative of the density  $\rho$  with respect to the total potential  $\Psi$ . The derivative is in units of  $(4\pi G_N)^{-2} \rho_s^{-1} r_s^{-4}$ . **Bottom panel:** Third derivative  $d^3\rho/d\Psi^3$  in units of  $(4\pi G_N)^{-3} \rho_s^{-3/2} r_s^{-6}$ .

The situation changes when baryons are added to the potential. Then the DFs flatten at high energy (toward the central regions), and may even turn into a dip, as is the case of the DM core ( $\gamma = 0$ , solid magenta line), which violates the stability criterion in Eq. (3.19). The derivative  $d^2\rho/d\Psi^2$  takes negative values in that case and the stability criterion in Eq. (3.22) is also violated as expected. This mass model is therefore very likely to correspond to an unstable phase-space configuration.<sup>3</sup> The presence of a dip in the ergodic DF has direct consequences in the speed distribution defined in Eq. (2.8). In the left panel of Fig. 7, we show

<sup>3</sup>More precisely, the initial assumption of ergodicity cannot accommodate this density-potential pair; one would need to increase the number of degrees of freedom in phase space to find a stable DF.



the speed distributions for the different mass models at  $r = 0.01$  kpc, *i.e.* corresponding to regions where the energy range probes the dip. The speed distribution of the unstable model (magenta line) exhibits a very strong double-peak feature: a very large peak at  $v \sim 450$  km/s, and a much smaller one at  $v \sim 50$  km/s. The phase-space distribution is somewhat artificially forced to large velocities to allow for a kinetic pressure strong enough to prevent the halo from collapsing to a cusp—hardly a stable configuration in the isotropic case. The appearance of such a double-peak feature is characteristic of a troublesome configuration, and we stress that it has to be checked all over the halo (equivalently all over the available energy range). Indeed, the same problematic model would have given a perfectly licit speed distribution at larger radii (where the energy range would not probe the dip in the DF). We note, however, that it is not straightforward to firmly analyze this feature in terms of instability since it is also present in the  $\gamma = 0.25$  case, which satisfies the stability criterion, while clearly exhibiting a transition to a double-peak distribution. This can be seen in the blue curve of Fig. 7. In fact, as can readily be guessed from Eq. (2.13) (the part in brackets) and from both the top right and the bottom panels of Fig. 6, a way to select better-behaved speed distributions (without double-peak feature) is simply to impose an additional criterion based on the third derivative instead of the second:

$$\frac{d^3\rho}{d\Psi^3} > 0, \quad \forall\Psi. \quad (3.24)$$

In the following, we will remain agnostic about the origin of this two-peak behavior and just stick to the stability criterion of Eq. (3.22), keeping in mind that Eq. (3.24) could further be applied to remove controversial cases. We therefore keep the McM17  $\gamma = 0.25$  case as viable, while we reject the  $\gamma = 0$  case.

We now wish to characterize in more detail the instability when baryons contribute to the potential. We write the mass of the system as  $m = m_D + m_B$  and the gravitational potential as  $\Psi = \Psi_D + \Psi_B$ . Then the derivative that appears in the stability criterion can be written

$$\frac{d^2\rho}{d\Psi^2} = \left(\frac{m_D}{m_D + m_B}\right)^2 \left[ \frac{d^2\rho}{d\Psi_D^2} - \frac{d\rho}{d\Psi_D} \frac{d}{d\Psi} \left(\frac{m_B}{m_D}\right) \right]. \quad (3.25)$$

From this expression, we get the sufficient condition for stability:

$$\frac{d^2\rho}{d\Psi_D^2} \Big/ \frac{d\rho}{d\Psi_D} > \frac{d}{d\Psi} \left(\frac{m_B}{m_D}\right). \quad (3.26)$$

The quantities appearing on the left-hand side of Eq. (3.26) only refer to DM, while baryons appear on the right-hand side through their mass  $m_B = m_B(r)$  and the total potential  $\Psi$ . In the absence of baryons,  $m_B = 0$  and Eq. (3.26) simplifies to  $d^2\rho/d\Psi_D^2 > 0$  which is exactly the stability criterion in the DM-only case. Let us discuss the right-hand term in more detail. The baryonic mass is present in the ratio  $m_B/m_D$  and in the potential  $\Psi$ , so we do not expect it to be the most important parameter here. Rather, the spatial extension of the baryonic distribution with respect to the DM one is the relevant factor. To illustrate this, we show the ratio  $m_B/m_D$  as a function of  $\Psi$  in the right panel of Fig. 7. We show the isolated contribution of the bulge and the disk, as well as the total baryonic contribution. We can see that the bulge-to-DM ratio is steeper than both the disk-to-DM and baryons-to-DM ratios. The bulge-only configuration is therefore more likely to be inconsistent with the

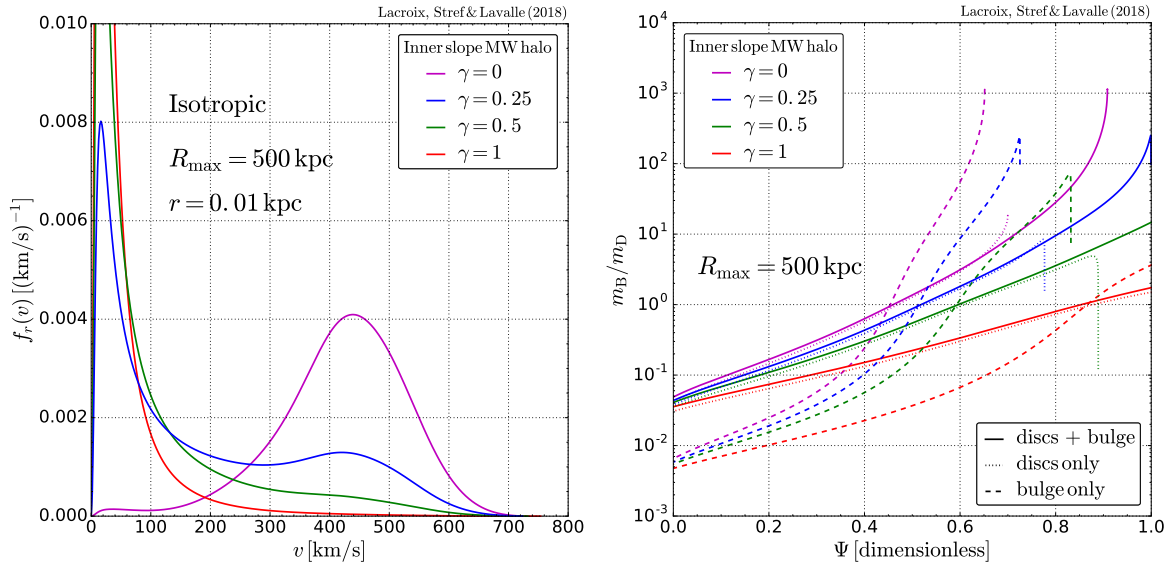


**Figure 7:** **Left panel:** Speed distribution at  $r = 0.01 \text{ kpc}$  for the mass models of [39], computed from the ergodic DF in Eq. (3.20). **Right panel:** Ratio of the baryonic mass to the DM mass as a function of the total potential  $\Psi$  (in units of  $4\pi G_N \rho_s r_s^2$ ).

ergodic assumption than the disk-only configuration and the full mass model, even though the baryonic mass is much less important in that case.

We also investigated the effects on the second derivative  $d^2\rho/d\Psi^2$  of changing the bulge characteristic mass density  $\rho_{0,b}$  and radius  $r_b$  (see Eq. A.1), while keeping the disks parameters fixed. Results are shown in Fig. 8, where we plot  $r_b/r_s$  as a function of  $\rho_{0,b}/\rho_s$ . The bulge parameters are scaled to the dark halo parameters. The points correspond to the McM17 mass models [39] for  $\gamma = 0, 0.25, 0.5$ . Those three models have nearly identical values for the bulge parameters, the difference in coordinates only comes from the change in the halo parameters  $\rho_s$  and  $r_s$ . The red shaded areas are the portions of parameter space where  $d^2\rho/d\Psi^2$  goes negative, *i.e.* the Eddington DF violates the stability criterion. We can see in Fig. 8 that the  $\gamma = 0$  mass model point is inside the  $\gamma = 0$  excluded area, while the  $\gamma = 0.25$  and  $\gamma = 0.5$  models are in their allowed regions. This is in agreement with the right panel of Fig. 6, where the  $\gamma = 0$  case is explicitly shown to violate the stability criterion. This figure further allows one to easily check whether one’s favorite Galactic mass model can be Eddington inverted.

### 3.2.3 Positive and stable distribution functions: summary

In this section, we have discussed several theoretical issues that arise when trying to infer the DF of a galactic system in a self-consistent way with the Eddington formalism and its most simple anisotropic extensions. We have established its validity range, and provided prescriptions to deal with these issues. These prescriptions can be readily used to ensure a self-consistent application of Eddington-like inversions.

We have first discussed in Sec. 3.2.1 the conditions to get a DF positive over the whole energy range—this is mostly relevant to systems with both DM and baryons. For a DM profile of the  $\alpha\beta\gamma$  type [see Eq. (A.5)], we isolated a rather simple necessary condition on the index  $\alpha$  given in Eq. (3.18), which forces the transition between the asymptotic indices  $\gamma$  and  $\beta$  to

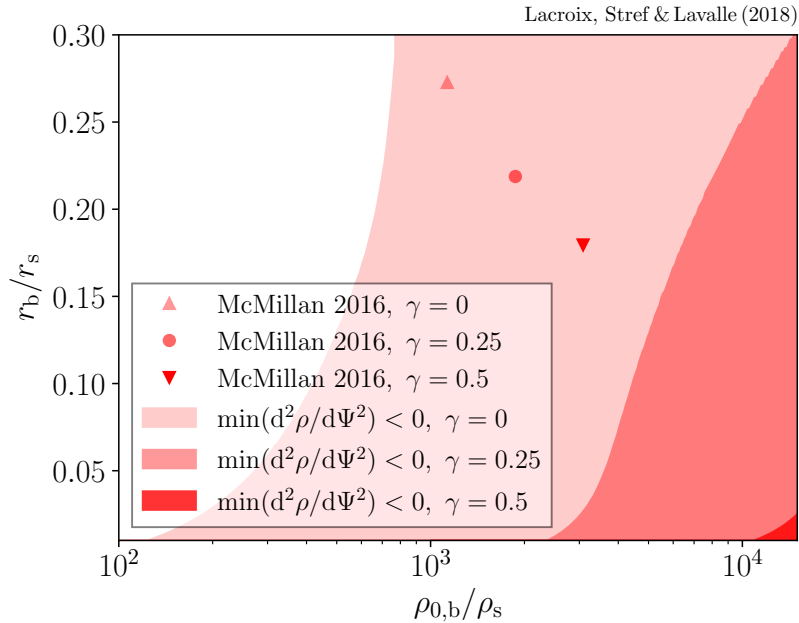


**Figure 8:** Sign of the minimum of  $d^2\rho/d\Psi^2$  on the plane  $(\rho_{0,b}/\rho_s, r_b/r_s)$  with  $\rho_{0,b}$  ( $\rho_s$ ) and  $r_b$  ( $r_s$ ) the characteristic density and radius of the bulge (dark halo). The parameters of the disk are fixed to the MCM17 values. Results are shown for  $\gamma = 0, 0.25, 0.5$  with  $\gamma$  the inner slope of the DM profile. Points indicate the positions of the McMillan models.

be smoother and smoother as the baryonic distribution steepens in the very central parts of the Galaxy—this also applies to the anisotropic Osipkov-Merritt model, which actually tends to the isotropic case when  $r \ll r_a$ . For constant-anisotropy models, a necessary condition exists in terms of  $\beta_0$ , given in Eq. (3.17).

We have then discussed in Sec. 3.2.2 more fundamental features which can be related to the (in)stability of gravitational systems. We have shown that the Eddington inversion can only provide a well-behaved DF when the condition given in Eq. (3.22) is fulfilled. An even more stringent condition providing an unambiguous speed distribution is given in Eq. (3.24). In contrast to the positivity issue though, stability conditions cannot be derived in the anisotropic cases, except for the very special case of radial perturbations. In that case, the stability conditions are given in Eq. (3.23).

Finally, we showed in Fig. 8 how to quickly check whether realistic Galactic mass models are Eddington-invertible, only from the bulge-to-halo ratio of the scale densities. This figure can be used as a preliminary diagnosis before going into more involved calculations. In any case, all the discussion developed in this section fully applies to the general case, for systems with or without baryons.

#### 4 Impact on predictions for dark matter searches

In this section, we study the impact of the issues discussed in the previous sections on predictions for DM searches. We shall obviously focus on velocity-dependent observables, and more particularly on observables related to both direct DM searches and indirect DM searches: the moments (and inverse moments) of the DM speed (relevant to direct DM searches, DM

capture by stars, or PBH microlensing), and the moments (an inverse moments) of the two-DM-particle relative speed (relevant to  $p$ -wave-suppressed or Sommerfeld-enhanced DM annihilation). We will embed the former observables in a *direct-search* class, while the latter will define the *indirect-search* class, to make more explicit contact with the WIMP phenomenology. We shall make quantitative comparisons between the self-consistent Eddington approach (whenever applicable) and the Maxwellian approximation, which is most commonly used in this context. Note that the Maxwell-Boltzmann (MB) DF or velocity distribution is consistent with the collisionless Boltzmann equation only if the underlying density profile is an infinite isothermal sphere that also dominates the potential. It is therefore by no means theoretically consistent with the input dark halo profile we will consider in the following calculations, but is usually assumed to provide a “reasonable” approximation. Like in the isothermal sphere, we will still use the link between the 3D velocity dispersion  $\sigma$  and the circular velocity as follows:

$$\sqrt{\frac{2}{3}} \sigma = v_{\text{circ}}(r) = \sqrt{\frac{G_{\text{N}} m(r)}{r}}, \quad (4.1)$$

with  $m(r)$  consistently derived from the mass model. Therefore, the dispersion velocity associated with the MB DF will be radial dependent in the following.

#### 4.1 Direct-search-like observables

Let us define a generic function for the moments of the DM speed in the Galactic frame:

$$\Xi_n(v_{\text{min}}, v_{\text{max}}, r) \equiv \omega^{-1}(r) \int_{v_{\text{min}} \leq |\vec{v}| \leq v_{\text{max}}} d^3\vec{v} |\vec{v}|^n f_{\vec{v}}(\vec{v}, r) \quad (4.2a)$$

$$\omega(r) \equiv \int d^3\vec{v} f_{\vec{v}}(\vec{v}, r), \quad (4.2b)$$

where  $f_{\vec{v}}(\vec{v}, r)$  is the velocity distribution in the Galactic frame, generically defined in the context of the Eddington inversion by Eq. (2.8), and  $\omega(r)$  ensures the normalization of the distribution to unity over the full available range in velocity [1 by construction in the Eddington formalism, except if some terms are neglected—see discussion below Eq. (2.14)].

Direct searches for WIMP dark matter are typically sensitive to the inverse moment of the velocity, expressed as the following integral:

$$\eta(v_{\text{min}}) = \int_{v_{\text{min}} \leq v \leq v_{\oplus} + v_{\text{esc}}} d^3\vec{v} \frac{f_{\vec{v},\oplus}(\vec{v})}{v}, \quad (4.3)$$

where  $f_{\vec{v},\oplus}$  is the WIMP velocity distribution in the rest frame of the Earth. The speed  $v_{\text{min}}$  is the minimal speed a DM particle must have to induce a detectable recoil in the detector. Consequently, low-threshold experiments are sensitive to the high-velocity tail of the distribution. For low-mass DM candidates (noted  $\chi$  for convenience), with masses much lower than the target nucleus mass, the minimal speed is  $v_{\text{min}} \propto 1/m_{\chi}$  and can be close to the maximal speed in the laboratory frame  $v_{\text{max}} = v_{\oplus} + v_{\text{esc}}$ , where the Earth speed in the Galactic frame  $v_{\oplus}$  is close to the Sun speed  $v_{\odot} \sim 240$  km/s. Giving an accurate description of the tail of the speed distribution in the Galactic frame is therefore critical, and the regularization of the divergence associated with  $R_{\text{max}}$  is crucial in this context. We compare the prediction of the self-consistent Eddington inversion to the MB approximation. In the context of direct

searches, the MB distribution in the Galactic frame is usually truncated at the escape speed [86], either sharply,

$$f_{\vec{v}}^{\text{shm}}(\vec{v}) = \frac{1}{N_{\text{shm}}} e^{-v^2/v_{\text{circ}}^2} \Theta(v_{\text{esc}} - v), \quad (4.4)$$

where  $\Theta$  is the Heaviside step function, or smoothly,

$$f_{\vec{v}}^{\widetilde{\text{shm}}}(\vec{v}) = \frac{1}{N_{\widetilde{\text{shm}}}} \left( e^{-v^2/v_{\text{circ}}^2} - e^{-v_{\text{esc}}^2/v_{\text{circ}}^2} \right). \quad (4.5)$$

The respective normalizations are  $N_{\text{shm}} = (\pi v_{\text{circ}}^2)^{3/2} [\text{erf}(z) - 2z/\sqrt{\pi} \exp(-z^2)]$  and  $N_{\widetilde{\text{shm}}} = (\pi v_{\text{circ}}^2)^{3/2} [\text{erf}(z) - 2z/\sqrt{\pi} (1 + 2z^2/3) \exp(-z^2)]$ , and  $z = v_{\text{esc}}/v_{\text{circ}}$ . Note that the sharply-cut MB distribution is obviously non-physical due to the step at  $v_{\text{esc}}$ . We consider it nonetheless since it has been used extensively in the direct searches literature. These deformed MB velocity distributions are usually dubbed *standard halo model* (SHM). In the following, we will pick the values of  $v_{\text{circ}}$  at  $r = R_{\odot}$  consistently with the McM17 models used in this study.

Our comparison of  $\eta$  for the various cases should not depend significantly on the frame of reference up to a Galilean shift in velocity, so for simplicity we consider the Galactic frame rather than the Earth frame (which is the frame relevant for direct searches)—our  $v_{\text{min}}$  should thereby be shifted by the Sun speed in the Galactic frame  $\sim v_{\odot}$  to get values more relevant to direct WIMP searches. We consider the McM17 NFW model for illustration (see Sec. A) and the different regularization methods discussed in Sec. 3.1, and assume

$$\eta(v_{\text{min}}) \simeq \Xi_{-1}(v_{\text{min}}, v_{\text{esc}}, R_{\odot}). \quad (4.6)$$

We compare the predictions inferred from the SHM and the Eddington inversion for  $\eta(v_{\text{min}})$  in the left and right panels of Fig. 9 for the isotropic and Osipkov-Merritt cases, respectively. Generically, predictions derived from the Eddington inversion differ significantly from that of the SHM over the whole range of  $v_{\text{min}}$ , as already noticed in the literature [25, 26, 30–32]—the main difference with previous studies comes from our rigorous treatment of the issues emphasized in Sec. 3, and the selection of stable configurations only. Differences are especially striking when  $v_{\text{min}}$  is large due to the different shapes predicted in the tail of the speed distribution. The smoothly-cut MB distribution is closer to the Eddington prediction than the sharply-cut MB distribution, but it is also very discrepant near  $v_{\text{esc}}$ . We also make the comparison with the Osipkov-Merritt models.<sup>4</sup> The difference between the SHM and these models are much larger than in the isotropic case. This is an illustration of the difficulty to regularize the Osipkov-Merritt models, for which none of the prescriptions are fully satisfactory (see Sec. 3.1). Either the divergence is not removed ( $R_{\text{max}} \rightarrow \infty$  case) or the underlying density profile is significantly modified.

Thus, irrespective of the regularization and the anisotropy, the prediction of the self-consistent approach systematically differs from the SHM. We are able to quantify the theoretical uncertainties associated with the treatment of the divergence, which is especially important for large values of  $v_{\text{min}}$ . This is critical for low-mass DM candidates in direct searches. For the sake of completeness, we also compare the Eddington inversion and MB results obtained for the observables proportional to  $\bar{\eta} \equiv \Xi_{-1}(0, v_{\text{max}}, r)$ , which could be related to the capture of DM in stars or planets (e.g. [87–93]), and to  $\langle v \rangle = \Xi_1(0, v_{\text{esc}}, r)$ , which

<sup>4</sup>We do not show the constant- $\beta$  case as the regularization is very similar to the isotropic case.

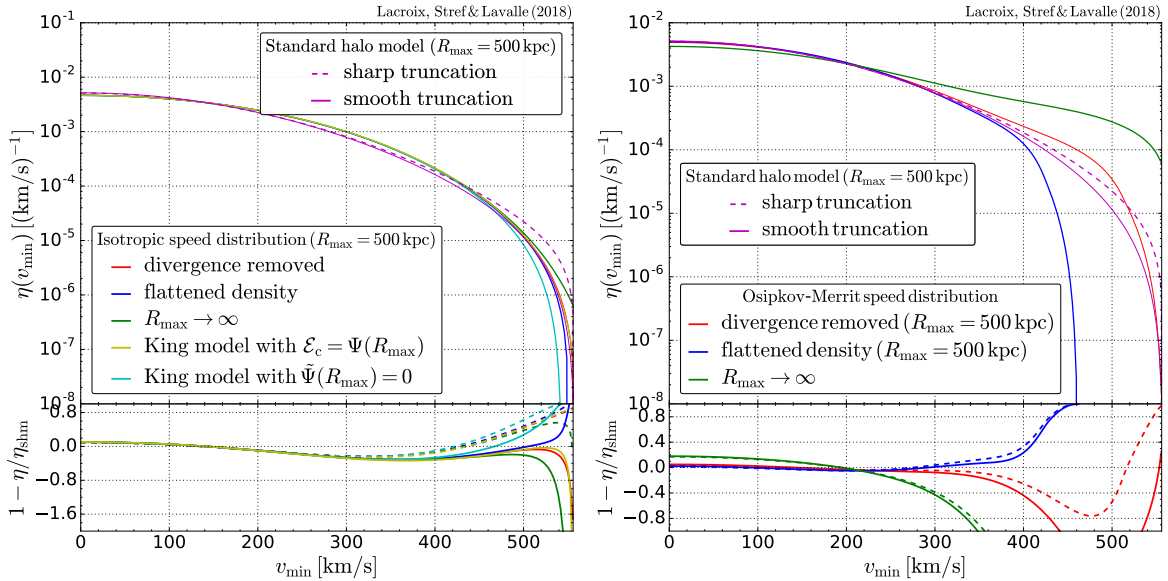


**Figure 9: Left panel:**  $\eta$  integral as a function of  $v_{\min}$ . The various curves shown are the sharply-cut SHM (solid magenta), the smoothly-cut SHM (dashed magenta), and the predictions of the Eddington formalism for an isotropic system, with the regularizations of the phase-space divergence discussed in Sec. 3.1, namely setting  $R_{\max}$  to infinity (green), removing the diverging term (red), modifying the density profile (blue), regularizing à la King with  $\mathcal{E}_c = \Psi(R_{\max})$  (yellow) or with  $\Psi(R_{\max}) = 0$  (cyan). **Right panel:** Same as left panel, for the Osipkov-Merritt model.

could be related to the microlensing event rate of compact DM objects (*e.g.* [94, 95])—the latter is simply the mean speed across the Galaxy.

Our results are illustrated in Figs. 10 and 11 for  $\bar{\eta}$  (for which we set  $r = R_{\odot}$ ) and  $\langle v \rangle$ , respectively. For  $\bar{\eta}$ , we see significant differences between the Eddington inversion and the Maxwellian approximation, decreasing from  $\sim 40\%$  to  $\sim 10\%$  as  $v_{\max}$  spans the full dynamical range—we also see that isotropic DFs are poorly sensitive to the radial cutoff treatment, in contrast to anisotropic DFs, where radial orbits come into play. For the mean speed  $\langle v \rangle$ , the only regions where the Maxwellian approximation provides results similar to the Eddington inversion are the outer parts of the Galaxy. The departure between the two prediction increases as the radius gets smaller, with up to an order of magnitude of difference at the center of the Galaxy. This should therefore be considered seriously in predictions of related observables. The negative  $\beta$  case leads to a mean speed curve closer to the Maxwellian case, as expected for more circular orbits (the mean speed then tends to the circular speed). Note that the Maxwellian results are obviously similar for all Galactic models when both the DM and baryons are included, as these models are constrained from rotation curves; they consequently separate from each other when only the DM halo is considered (the DM mass profiles may vary significantly in regions dominated by the baryons). The results obtained for the moments of the relative speed in Sec. 4.2 exhibit the same behavior.

## 4.2 Indirect-search-like observables

Other DM-related signals are related to moments (or inverse moments) of the relative speed instead of the speed. This concerns signals related to two-body processes, whose most striking example is the self-annihilation of DM. We therefore define a new moment function for the

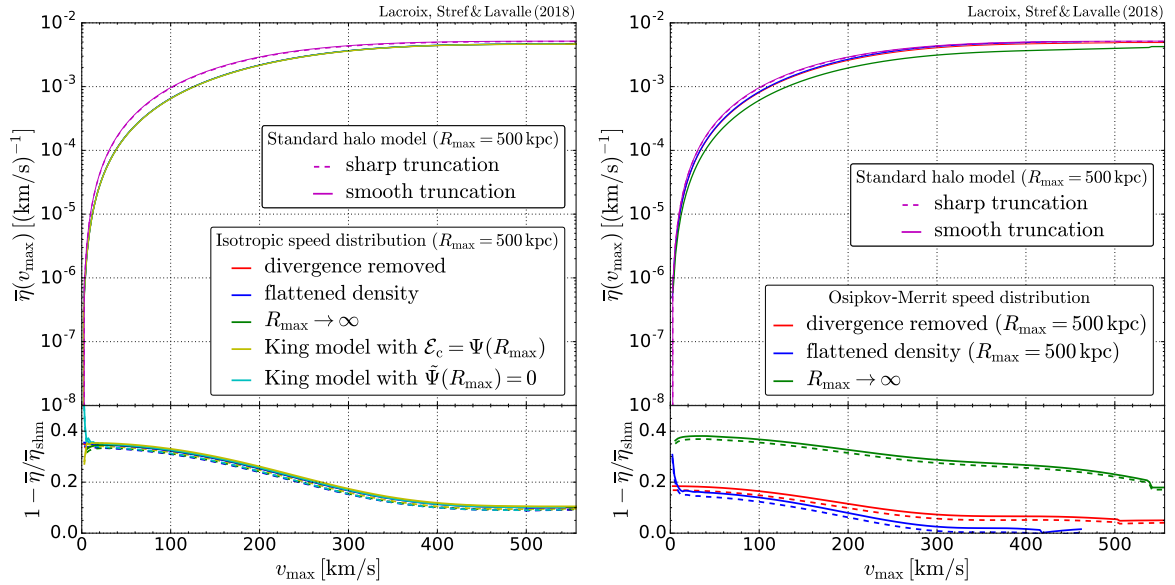


**Figure 10:** Same as Fig. 9 for  $\bar{\eta} \equiv \Xi_{-1}(0, v_{\max}, R_{\odot})$ .

relative speed  $\vec{v}_r = \vec{v}_2 - \vec{v}_1$  between two DM particles,

$$\Pi_n(v_{\min}, v_{\max}, r) \equiv \kappa^{-1}(r) \int_{v_{\min}}^{v_{\max}} d^3 \vec{v}_1 \int_{v_{\min}}^{v_{\max}} d^3 \vec{v}_2 |\vec{v}_r|^n f_{\vec{v}}(\vec{v}_1, r) f_{\vec{v}}(\vec{v}_2, r) \quad (4.7a)$$

$$\kappa(r) \equiv \int d^3 \vec{v}_1 \int d^3 \vec{v}_2 f_{\vec{v}}(\vec{v}_1, r) f_{\vec{v}}(\vec{v}_2, r), \quad (4.7b)$$

where the velocity distribution  $f_{\vec{v}}$  is conventionally defined by Eq. (2.8) in the context of Eddington’s inversion formalism, and the function  $\kappa(r)$  ensures the correct normalization to unity in the relevant range of individual speed [1 by construction in the Eddington formalism, except if some terms are neglected—see discussion below Eq. (2.14)].

Indirect searches for self-annihilating DM are sensitive to the following moments

$$\langle |\vec{v}_r|^n \rangle(r) = \Pi_n(0, v_{\text{esc}}, r) \quad (4.8)$$

Searches for  $p$ -wave annihilation typically probe the (relative) velocity dispersion ( $n = 2$ ), though in some interaction models the annihilation cross-section can be modified by non-perturbative effects [96] that lead to the so-called Sommerfeld enhancement, which induces a dependency on the  $n = -1$  moment—as well as the  $n = -2$  moment at resonances. Note that in practice it proves convenient to perform the following change of variable to express the integrals in terms of the center-of-mass velocity  $\vec{v}_c$  and relative velocity  $\vec{v}_r$  (e.g. [97]):

$$\begin{cases} \vec{v}_c = (\vec{v}_1 + \vec{v}_2)/2 \\ \vec{v}_r = \vec{v}_2 - \vec{v}_1. \end{cases} \quad (4.9)$$

As a result, Eq. (4.8) can be rewritten

$$\langle v_r^n \rangle = \int d^3 \vec{v}_r |\vec{v}_r|^n F_r(\vec{v}_r, r), \quad (4.10)$$

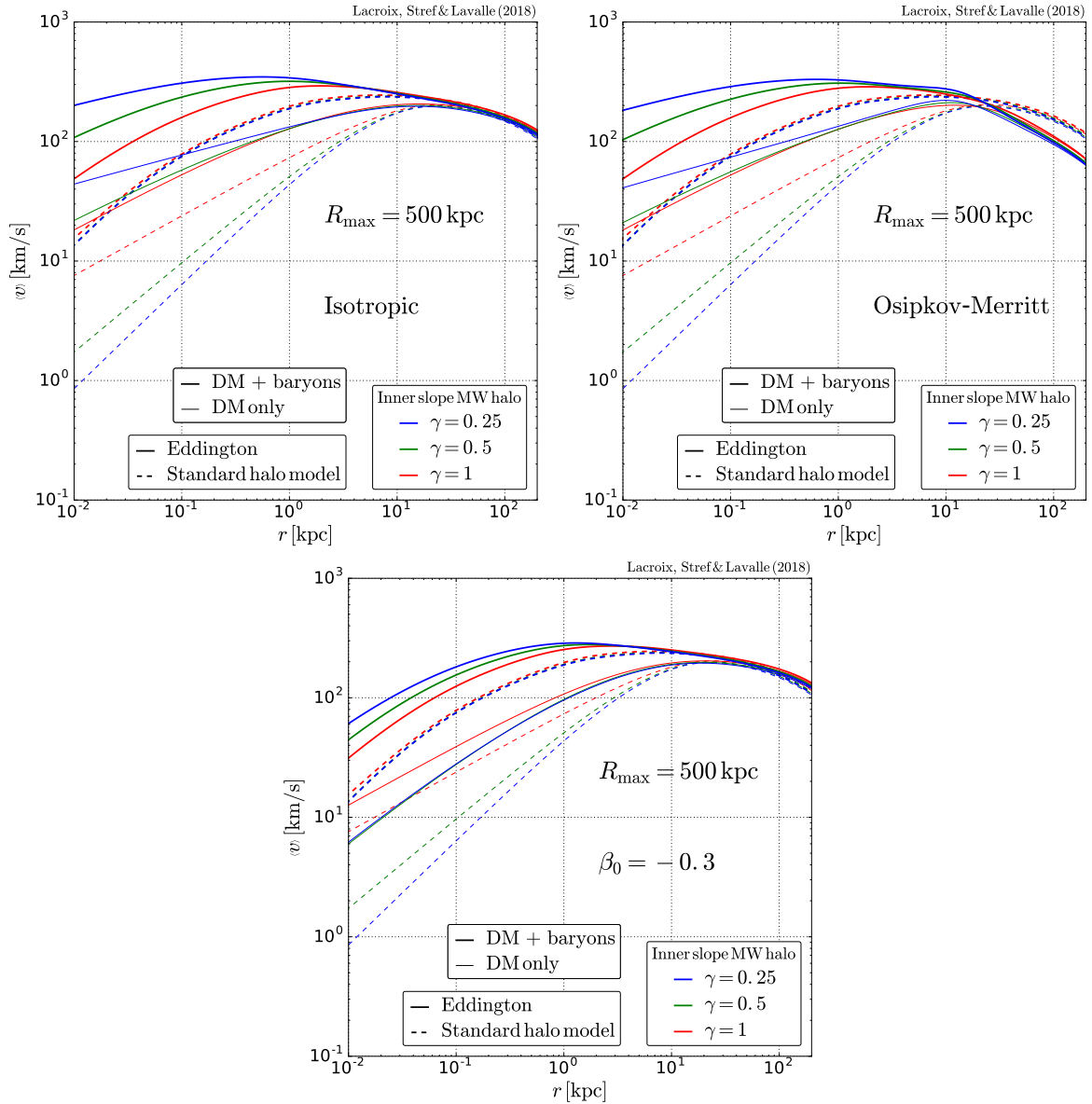


**Figure 11:** Mean speed profiles for the Standard Halo Model and the Eddington formalism for the isotropic (top left panel), Osipkov-Merritt (top right panel) and  $\beta_0 = -0.3$  (bottom panel) cases. Here we show the DM-only (thin line) and DM+baryons (thick line) cases, for the McM17 mass models providing well-behaved Eddington-inverted DFs.

where  $F_r$  is the relative velocity DF, which is defined as

$$F_r(\vec{v}_r, r) \equiv \kappa^{-1}(r) \int d^3\vec{v}_c f_{\vec{v}}(\vec{v}_1, r) f_{\vec{v}}(\vec{v}_2, r). \quad (4.11)$$

The full derivation of  $F_r(\vec{v}_r, r)$  is given in App. B in the Eddington formalism and its anisotropic extensions discussed above. To our knowledge, the computation of  $F_r(\vec{v}_r, r)$  in the general anisotropic case is an original result. An alternative treatment for the Osipkov-Merritt models is presented in Ref. [36].



We show the predictions for the relative speed moments inferred from the (smoothly-truncated) SHM and the isotropic Eddington inversion in Fig. 12. Following our discussion regarding the stability of the DFs, we only consider here mass models leading to stable solutions of the Boltzmann equation. The velocity distribution in the Eddington case have been computed *without* the diverging term, *i.e.* using Eq. (3.20). We recall that this is in practice similar to assuming a flattened density profile at the outskirts of the halo, as in Eq. (3.2). One can see in Fig. 12 that, for both the SHM and the Eddington model, the moments with and without baryons converge at large radii. This is because the total mass, and therefore the gravitational dynamics, is then fully dominated by DM, and baryons become irrelevant. Though similar in shape, predictions from the two models are numerically quite different. For the  $n > 0$  moments, the Eddington model’s predictions typically exceed the SHM’s. At the center of the Galaxy, the two models differ by at least an order of magnitude, up to three orders of magnitude. The hierarchy of the moments with respect to the value of DM inner slope  $\gamma$  is also reverted. While the cuspiest mass model ( $\gamma = 1$ ) leads to the largest prediction for the SHM, it is the model closest to the core ( $\gamma = 0.25$ ) that dominates the Eddington result. We stress that even locally at  $r = R_\odot \sim 8$  kpc, and for all  $n$ , there are sizable differences between the Eddington formalism and the Maxwell-Boltzmann approximation. Therefore, since the Eddington formalism turns out to better capture the dynamical properties of the DM halo than the SHM [21], the latter should only be used to make very rough estimates of  $p$ -wave annihilating DM signals, even when isotropy is assumed.

We also compared the (isotropic) SHM with some of the anisotropic extensions of the Eddington formalism. The prediction of the Osipkov-Merritt model is shown in Fig. 13 for a particular choice of the anisotropy radius  $r_a = r_s$ . Note that the value of  $r_s$  depends on the underlying mass model (see Tab. 1). The result is close to the isotropic case at radii  $r \ll r_a$ , as expected from the behavior of the anisotropy parameter Eq. (2.23). At large radii however, the slope of the moments steepens significantly. The steepening starts roughly where  $r \simeq r_a$  which is where the system begins to be strongly anisotropic. We stress again the fact the regularization of the diverging term changes considerably the underlying density profile in the Osipkov-Merritt case, as seen from Fig. 4. The behavior of  $\langle v_r^n \rangle$  beyond  $r = r_a$  should therefore be treated with caution. We also studied the constant anisotropy case, focusing on  $\beta_0 = -0.3$ . We considered a negative anisotropy to get a well-defined DF for all the mass models of relevance here. The corresponding relative speed moments are shown in Fig. 14. They differ from the isotropic ones at all radii, unlike the Osipkov-Merritt ones, which is not surprising since the constant anisotropy is non zero everywhere.

Regardless of the assumption made on the anisotropy, the Eddington formalism generically predicts huge differences with respect to the SHM. The various anisotropic models we used allow us to bracket the theoretical uncertainty on the Eddington method.

## 5 Conclusion

In this paper, we have reviewed the Eddington inversion formalism, and a few of its generic extensions to anisotropic systems. This formalism is powerful to consistently include the dynamical correlations featured by a self-gravitating system in the DM-search-related velocity-dependent observables, from a mass model constrained on real data. It represents a strong improvement over the Maxwellian approximation from both the theoretical and quantitative points of view, and should therefore become a “next-to-minimal” standard approach to refine the predictions and better quantify the dynamical uncertainties in DM-search predictions

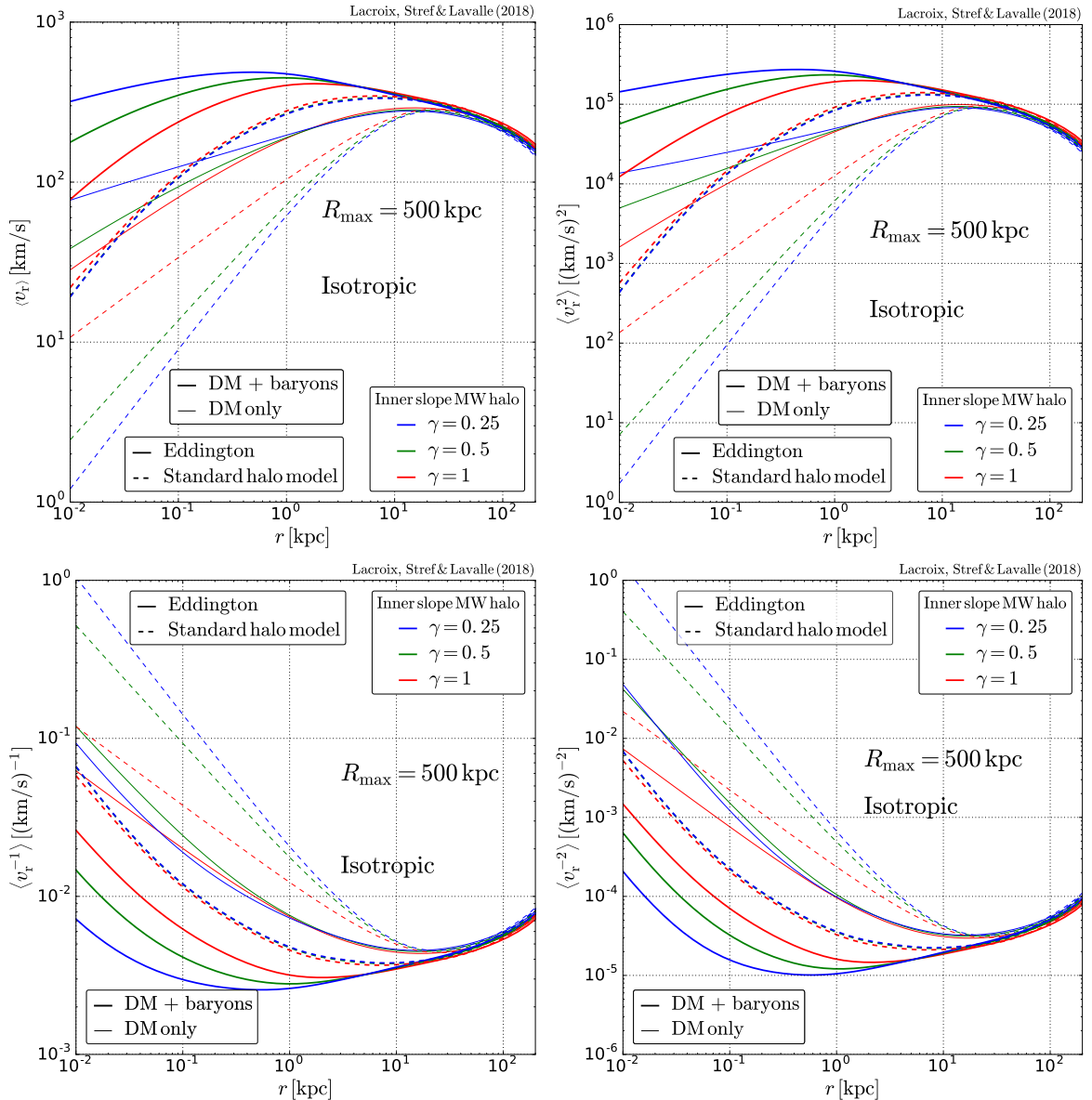


**Figure 12:** Moments of the relative velocity distribution, for the Standard Halo Model and the Eddington formalism (isotropic case). Here we show the DM-only (thin line) and DM+baryons (thick line) cases, for several mass models from Ref. [39].

pertaining to (sub)Galactic scales. It is also more appealing theoretically than blindly using ad-hoc fits from cosmological simulations, which likely hide environmental dependencies or other artifacts. Though not as evolved nor as adaptable to a large variety of potential-density pairs as the action-angle formalism [48], Eddington’s inversion method still provides a decent description of galactic DM halos [21] from a minimal set of physical assumptions and a moderate level of technicalities—pending the breakdown of some assumptions (*e.g.* spherical symmetry, steady state, smoothness of the dark halo, *etc.*) that induces additional systematic errors which remain to be quantified. Inspecting the self-consistency of this approach is therefore particularly important at the time of a boost in astrometric precision made possible

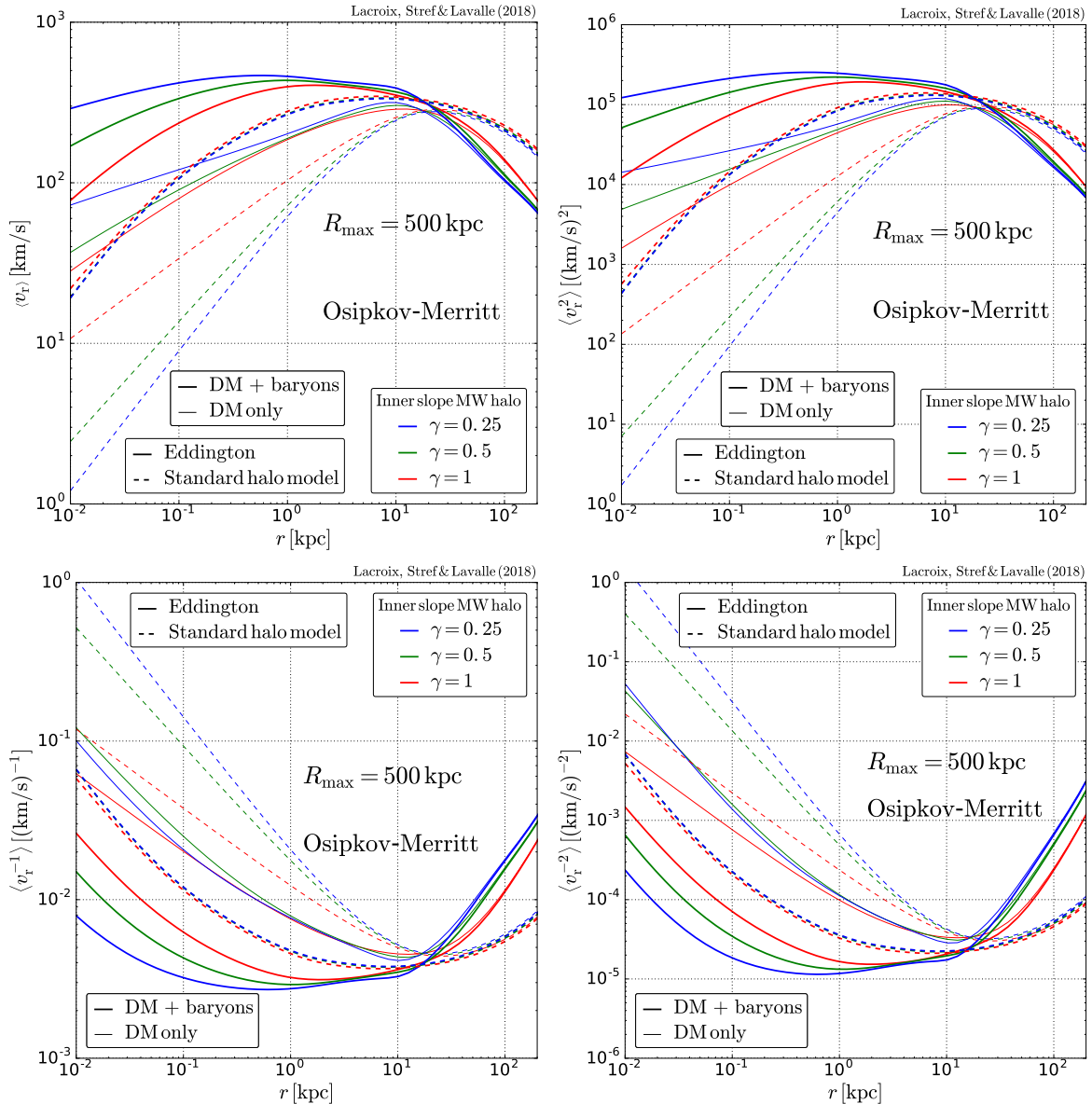


**Figure 13:** Same as Fig. 12, for the Osipkov-Merritt model with  $r_a = r_s$ .

by the Gaia mission [12], which should provide much better constraints on the DM content of the MW and its satellites. This is of special relevance in the context of intense DM searches, as the Eddington-like inversion methods are well suited to better control and further reduce the astrophysical uncertainties in the signal predictions—*e.g.* in direct [25, 27, 31], indirect [33–36], or combined [16] WIMP searches, but not only.

After carefully inspecting the Eddington inversion formalism in Sec. 2, however, we noticed several theoretical issues related to (i) the radial boundary of the dark halo, important to make sense of the constraints on the escape speed [32], and (ii) to the stability of the phase-space DF, which have been overlooked in the DM-related literature, but which are actually expected to arise very often when Eddington inverting Galactic mass models with a baryonic component. We have described and addressed these issues in Sec. 3, and

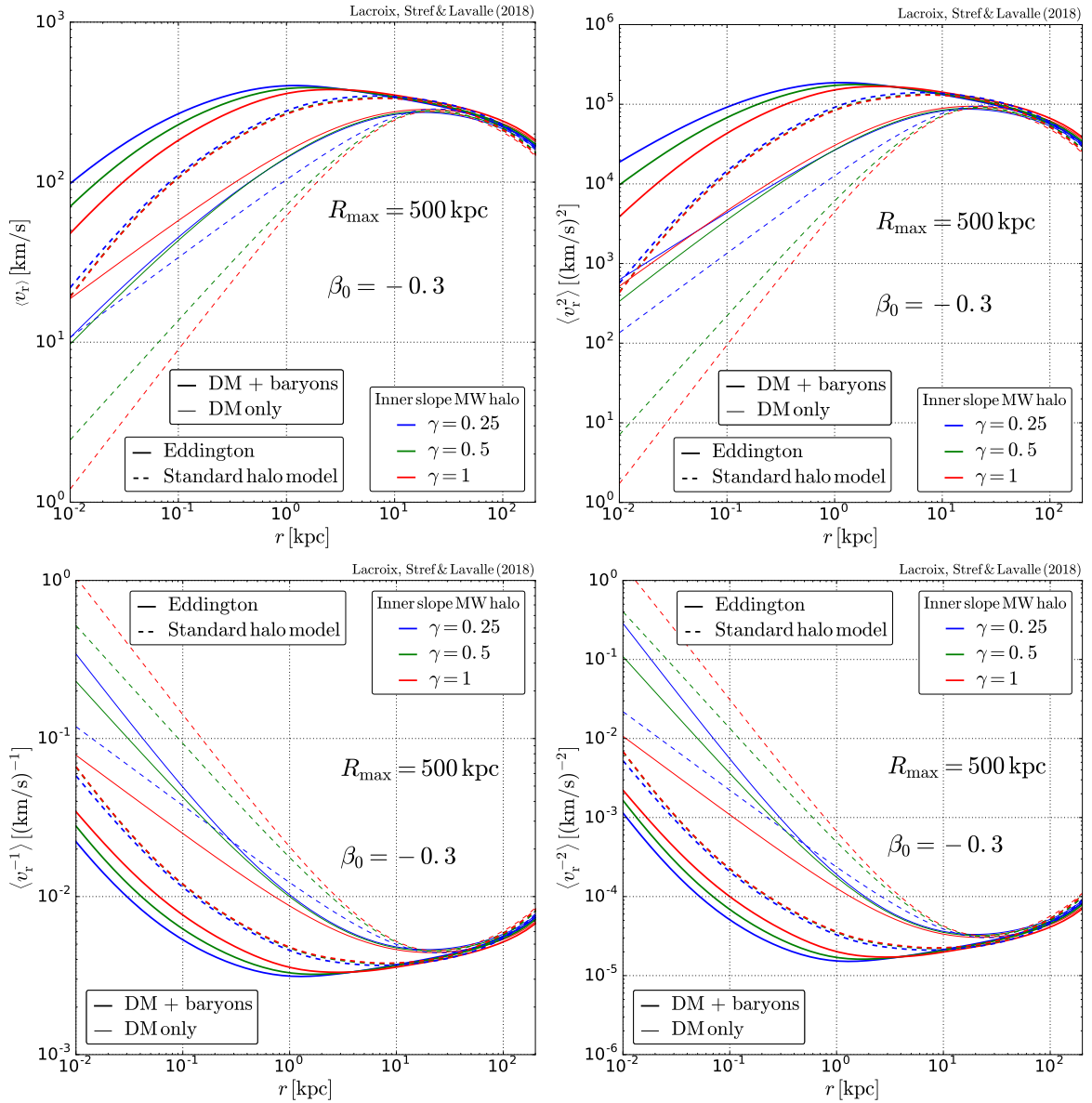


**Figure 14:** Same as Fig. 12, for the constant- $\beta$  model with  $\beta_0 = -0.3$ .

provided generic methods to cure some of the potential inconsistencies. For the divergence induced in the phase-space DF in the limit of  $v \rightarrow v_{\text{esc}}$  (see Sec. 3.1), after explaining why the diverging term  $\propto 1/\sqrt{\mathcal{E}}$  should actually not be dropped, we defined two ways of getting a non-anomalous phase-space DF without spoiling too much the initial mass model, based either on *a priori* modifications of the DM profile or on new converging ansätze for the DF itself. Properly describing the boundary of the system is particularly important to characterize the theoretical uncertainties affecting DM-search observables depending on the high-velocity tail of the DM velocity distribution, like the direct detection rate of GeV- or subGeV-mass WIMPs. The proposed regularization methods proved efficient in all cases, except in the case of the anisotropic Osipkov-Merritt model, which cannot consistently accommodate radial boundaries. As for the stability issue (see Sec. 3.2), we recovered stability criteria for

both the isotropic case [see Eq. (3.22)] and the anisotropic case [see Eq. (3.23), a criterion for stability against radial perturbations only]. The former criterion could be complemented by Eq. (3.24) to ensure a smoother velocity distribution, while this restricts the phase-space volume beyond the requirement of stability only. We also analyzed these stability conditions to get selection criteria for a Galactic halo based on its relative baryonic content—see Eq. (3.26) and Fig. 8. This allows one to quickly check whether one’s favorite Galactic mass model is Eddington invertible or not. The main conclusion of this part is that Eddington’s inversion (and its anisotropic extensions) cannot blindly apply to any density-potential pair. Particular attention should be given to moderately cuspy or cored halo profiles, which are more likely to exhibit ill-defined DFs.

Finally, we have explicitly computed some DM-search velocity-dependent observables to explicitly compare the Eddington inversion predictions with those derived in the Maxwellian approximation, in the framework of the McM17 constrained Galactic mass models [39]. In particular, we have computed observables that depend on the speed moments (and inverse moments), and on the relative speed moments (and inverse moments). The former ones regard the direct WIMP detection rate, and the latter ones regard  $p$ -wave self-annihilation of DM. For the self-annihilation case, we have derived a convenient way to express the relative velocity distribution function for anisotropic systems, reviewed in App. B. We have seen that the differences are quite sizable in all observables, which somewhat quantifies the associated level of theoretical uncertainties. We will actually show in a forthcoming study that the Eddington inversion methods provide a significantly better description of the true DF than the Maxwellian approximation in zoomed-in cosmological simulations with baryons [21]. This further motivates applications of this approach to exploit the upcoming Gaia-constrained mass models in the context of DM searches.

## Acknowledgments

The PhD grant of MS is funded by the OCEVU Labex (ANR-11-LABX-0060), which also provided financial support to this project. We also benefited from financial support from the theory project *Galactic Dark Matter* funded by CNRS-IN2P3. We further acknowledge support from the European Union’s Horizon 2020 research and innovation program under the Marie Skłodowska-Curie grant agreements No 690575 and No 674896; beside recurrent institutional funding by CNRS-IN2P3 and the University of Montpellier.

## A Galactic mass models used in this study

For definiteness, we used a selection of mass models from Ref. [39] (the McM17 model henceforth), featuring a stellar bulge, two stellar disks, two gas disks and a DM halo. The bulge profile reads

$$\rho_{\text{b}} = \frac{\rho_{0,\text{b}}}{(1 + r'/r_0)^\alpha} \exp \left[ - (r'/r_{\text{b}})^2 \right], \quad (\text{A.1})$$

where

$$r' = \sqrt{R^2 + (z/q)^2}. \quad (\text{A.2})$$

**Table 1:** Dark matter mass models from Ref. [39].

$(\alpha, \beta, \gamma)$	$\rho_s$ [ $M_\odot/\text{kpc}^3$ ]	$r_s$ [kpc]	$\rho_\odot$ [ $M_\odot/\text{kpc}^3$ ]	$R_\odot$ [kpc]
(1, 3, 0)	$9.09 \times 10^7$	7.7	$1.03 \times 10^7$	8.21
(1, 3, 0.25)	$5.26 \times 10^7$	9.6	$1.01 \times 10^7$	8.20
(1, 3, 0.5)	$3.19 \times 10^7$	11.7	$1.01 \times 10^7$	8.21
(1, 3, 1)	$8.52 \times 10^6$	19.6	$1.01 \times 10^7$	8.21

The variable  $q$  determines the oblateness of the bulge,  $\rho_{0,b}$  is a scale density, and  $r_0$  and  $r_b$  are scale lengths. The stellar disks are modeled by exponential profiles:

$$\rho_{*,d}(R, z) = \frac{\Sigma_0}{2z_d} \exp\left(-\frac{|z|}{z_d} - \frac{R}{R_d}\right), \quad (\text{A.3})$$

with scale height  $z_d$ , scale length  $R_d$  and central surface density  $\Sigma_0$ . The HI and H<sub>2</sub> gas disks are described by

$$\rho_{g,d}(R, z) = \frac{\Sigma_0}{4z_d} \exp\left(-\frac{R_m}{R} - \frac{R}{R_d}\right) \text{sech}^2(z/2z_d). \quad (\text{A.4})$$

Finally, the DM halo is characterized by a generalized  $\alpha\beta\gamma$  profile [98]

$$\rho_{\text{DM}}(x) = \rho_s x^{-\gamma} (1 + x^\alpha)^{(\gamma-\beta)/\alpha} \quad (\text{A.5})$$

with  $x = r/r_s$ , where  $r_s$  is the scale radius. An NFW profile is recovered with  $(\alpha, \beta, \gamma) = (1, 3, 1)$ . The author of Ref. [39] uses instead  $\alpha = 1$  and  $\beta = 3$ , and fits the data for specific values of  $\gamma$ . For completeness, we also give the NFW gravitational potential:

$$\phi_{\text{NFW}}(r) = -4\pi G \rho_s r_s^2 x^{-1} \ln(1 + x). \quad (\text{A.6})$$

The best-fit parameters for the McM17 model are given in Tables 1 and 2.

## B Relative velocity distribution function

Here we provide the full derivation of the moments of the relative speed relevant for DM observables involving two-body processes. The  $n^{\text{th}}$  moment reads

$$\langle v_r^n \rangle = \int d^3\vec{v}_r |\vec{v}_r|^n F_r(\vec{v}_r, r), \quad (\text{B.1})$$

where the relative velocity distribution function at Galactic radius  $r$  already introduced in Eq. (4.11) is expressed as an integral over the center-of-mass velocity as follows:

$$F_r(\vec{v}_r, r) = \kappa^{-1}(r) \int d^3\vec{v}_c f_{\vec{v}}(\vec{v}_1, r) f_{\vec{v}}(\vec{v}_2, r). \quad (\text{B.2})$$

The normalization function  $\kappa(r)$  has been defined in Eq. (4.7).

**Table 2:** Baryonic mass model from Ref. [39], for the NFW DM profile ( $\gamma = 1$ , see Tab. 1).

	Parameter	Value
Bulge	$\rho_{0,b}$	$9.84 \times 10^{10} M_{\odot} \text{kpc}^{-3}$
	$r_{0,b}$	0.075 kpc
	$r_b$	2.1 kpc
	$q$	0.5
	$\alpha$	1.8
Stellar disks	$\Sigma_{0,\text{thin}}$	$8.96 \times 10^8 M_{\odot} \text{kpc}^{-2}$
	$R_{d,\text{thin}}$	2.5 kpc
	$z_{d,\text{thin}}$	0.3 kpc
	$\Sigma_{0,\text{thick}}$	$1.83 \times 10^8 M_{\odot} \text{kpc}^{-2}$
	$R_{d,\text{thick}}$	3.02 kpc
	$z_{d,\text{thick}}$	0.9 kpc
Gas disks	$\Sigma_{0,\text{HI}}$	$5.31 \times 10^7 M_{\odot} \text{kpc}^{-2}$
	$R_{d,\text{HI}}$	7 kpc
	$R_{m,\text{HI}}$	4 kpc
	$z_{d,\text{HI}}$	0.085 kpc
	$\Sigma_{0,\text{H}_2}$	$2.18 \times 10^9 M_{\odot} \text{kpc}^{-2}$
	$R_{d,\text{H}_2}$	1.5 kpc
	$R_{m,\text{H}_2}$	12. kpc
	$z_{d,\text{H}_2}$	0.045 kpc

### B.1 Isotropic system

For an isotropic system,  $f_{\vec{v}}(\vec{v}) = f_v(v)$ . Going from  $\vec{v}_1$  and  $\vec{v}_2$  to center-of-mass and relative velocities,

$$\begin{cases} \vec{v}_c = (\vec{v}_1 + \vec{v}_2)/2 \\ \vec{v}_r = \vec{v}_2 - \vec{v}_1, \end{cases} \quad (\text{B.3})$$

one can write

$$\langle v_r^n \rangle = 8 \pi^2 \int_{v_r^{\min}}^{v_r^{\max}} dv_r v_r^2 F_r(\vec{v}_r, r) \vec{v}_r^n. \quad (\text{B.4})$$

Let us define the angle

$$\theta \equiv (\vec{v}_c, \vec{v}_r) \quad (\text{B.5a})$$

$$\text{and } \mu \equiv \cos \theta. \quad (\text{B.5b})$$

From Eq. (B.3), we get

$$\begin{cases} \vec{v}_1 = \vec{v}_c - \frac{\vec{v}_r}{2} \\ \vec{v}_2 = \vec{v}_c + \frac{\vec{v}_r}{2}, \end{cases} \quad (\text{B.6})$$

hence the associated moduli

$$v_1 = |\vec{v}_1| = \sqrt{v_c^2 + \frac{v_r^2}{4} - v_c v_r \mu} \quad (\text{B.7a})$$

$$v_2 = |\vec{v}_2| = \sqrt{v_c^2 + \frac{v_r^2}{4} + v_c v_r \mu}. \quad (\text{B.7b})$$

In the Galactic frame, we have  $v_1 \leq v_{\text{esc}}$ , which gives the lower and upper bounds on  $\mu$ ,  $|\mu| \leq \mu_0$ , where

$$\mu_0(r, v_r, v_c) = \frac{v_{\text{esc}}^2 - v_c^2 - v_r^2/4}{v_c v_r}. \quad (\text{B.8})$$

Eq. (B.3) also implies that  $0 \leq v_c \leq v_{\text{esc}}$  and  $0 \leq v_r \leq 2v_{\text{esc}}$ .

Finally, we note that the product  $f_{\vec{v}}(\vec{v}_1, r) f_{\vec{v}}(\vec{v}_2, r)$  is conserved in the transformation  $\mu \rightarrow -\mu$ . Thanks to this symmetry, it is sufficient to perform the integral over  $\mu$  between 0 and  $\mu_0$ .

The final expression for the relative velocity DF is therefore

$$F_r(\vec{v}_r, r) = 4\pi\kappa^{-1}(r) \int_0^{v_{\text{esc}}} dv_c v_c^2 \int_0^{\mu_0} d\mu f_{\vec{v}}(v_1, r) f_{\vec{v}}(v_2, r), \quad (\text{B.9})$$

If  $f_{\vec{v}}(\vec{v}, r)$  is determined self-consistently and normalized to 1 by construction, then the normalization function  $\kappa(r) = 1$ . However, when modifying the DF, typically to account for the divergence discussed in Sec. 3.1, one needs to compute  $\kappa(r)$  for each value of  $r$  and renormalize the relative velocity DF by hand.

One can also define the distribution function for the relative speed  $v_r = |\vec{v}_r|$ . For an isotropic system, this reads

$$F_r^{1D}(v_r, r) = 4\pi v_r^2 F_r(\vec{v}_r, r). \quad (\text{B.10})$$

This allows one to readily compute the average of any observable  $\mathcal{O}(v_r)$  via

$$\langle \mathcal{O} \rangle_{v_r}(r) = \kappa^{-1}(r) \int_0^{2v_{\text{esc}}(r)} dv_r F_r^{1D}(v_r, r) \mathcal{O}(v_r). \quad (\text{B.11})$$

## B.2 Anisotropic extensions

For an anisotropic system, the DF no longer depends on the position and velocity only, but it also depends on the modulus of the angular momentum,  $L$ :  $f \equiv f(v, L, r)$ . In this case, it is still convenient to perform a change of variables from  $\vec{v}_1, \vec{v}_2$  to  $\vec{v}_c, \vec{v}_r$ , provided one uses the appropriate coordinate systems to describe the quantities of interest.

The anisotropy of the system is characterized by the specific direction defined by the radial unit vector  $\vec{e}_r$ . Physically, the outer integral on  $\vec{v}_c$  is equivalent to fixing  $v_c = |\vec{v}_c|$  and defining the angle

$$\alpha_c \equiv (\vec{v}_c, \vec{e}_r) \quad (\text{B.12})$$

in the coordinate system associated with  $\vec{e}_r$ , which is illustrated in the left panel of Fig. 15. Once  $\vec{v}_c$  is fixed, the system is invariant under any rotation about  $\vec{e}_r$ , so the associated angular integral directly gives a factor  $2\pi$ .



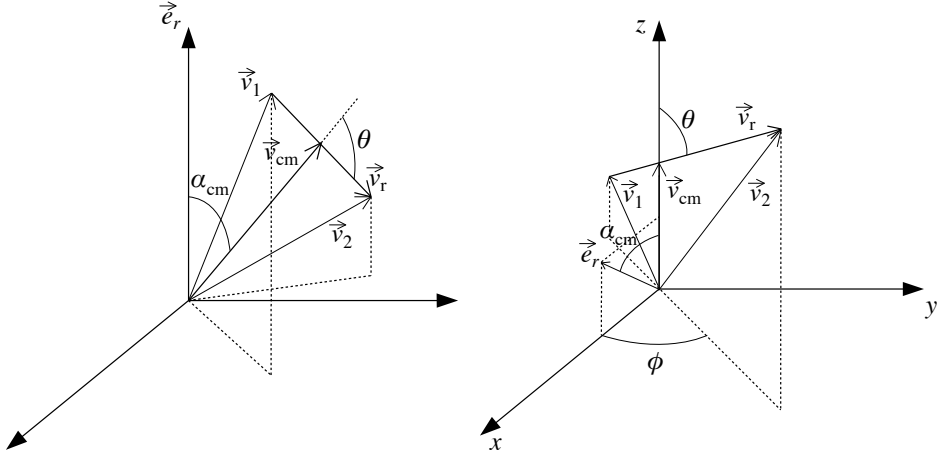


**Figure 15:** Coordinate systems for the derivation of the relative velocity DF for an anisotropic system. **Left panel:** Frame associated with  $\vec{r}$ , in which we define  $\vec{v}_c$ . **Right panel:** Coordinate system associated with  $\vec{v}_c$ .

To define  $\vec{v}_r$ , we then use the frame defined by  $\vec{v}_c$ , illustrated in the right panel of Fig. 15. There is no loss of generality by assuming that  $\vec{e}_r$  is orthogonal to  $\vec{e}_y$ . Therefore, in this frame, the vectors of interest read

$$\vec{v}_c = v_c \vec{e}_z, \quad (\text{B.13a})$$

$$\vec{e}_r = \cos \alpha_c \vec{e}_z + \sin \alpha_c \vec{e}_x, \quad (\text{B.13b})$$

$$\vec{v}_r = v_r (\cos \theta \vec{e}_z + \sin \theta \cos \phi \vec{e}_x + \sin \theta \sin \phi \vec{e}_y). \quad (\text{B.13c})$$

In the frame fixed by  $\vec{v}_c$ , the situation is the same as in the isotropic case, and we can use the integral bounds derived in the previous section. The DF for the modulus of the relative velocity is then given by

$$F_r^{1D}(v_r, r) = 2\pi \kappa^{-1}(r) v_r^2 \int_0^{v_{\text{esc}}} dv_c v_c^2 \int_{-1}^1 d\mu_c \int_0^{2\pi} d\phi \int_{-\mu_0}^{\mu_0} d\mu f_{\vec{v}}(v_1, L_1, r) f_{\vec{v}}(v_2, L_2, r), \quad (\text{B.14})$$

where  $\mu_c = \cos \alpha_c$  and  $\mu = \cos \theta$ . The velocity moduli  $v_1$  and  $v_2$  are defined in Eq. (B.7), and

$$\begin{aligned} L_1^2 &= \left| \vec{r} \times \left( \vec{v}_c - \frac{\vec{v}_r}{2} \right) \right|^2 \\ &= r^2 \left[ \frac{v_r^2}{4} (1 - \mu^2) \sin^2 \phi + \left\{ -\frac{v_r}{2} \mu_c \sqrt{1 - \mu^2} \cos \phi - \sqrt{1 - \mu_c^2} (v_c - \frac{v_r}{2} \mu) \right\}^2 \right], \end{aligned} \quad (\text{B.15a})$$

$$\begin{aligned} L_2^2 &= \left| \vec{r} \times \left( \vec{v}_c + \frac{\vec{v}_r}{2} \right) \right|^2 \\ &= r^2 \left[ \frac{v_r^2}{4} (1 - \mu^2) \sin^2 \phi + \left\{ \frac{v_r}{2} \mu_c \sqrt{1 - \mu^2} \cos \phi - \sqrt{1 - \mu_c^2} (v_c + \frac{v_r}{2} \mu) \right\}^2 \right]. \end{aligned} \quad (\text{B.15b})$$

## References

- [1] J. L. Feng, *Dark Matter Candidates from Particle Physics and Methods of Detection*, *Ann. Rev. Astron. Astrophys.* **48** (Sept., 2010) 495–545, [[1003.0904](#)].

- [2] J. Lavallo and P. Salati, *Dark matter indirect signatures*, *Comptes Rendus Physique* **13** (July, 2012) 740–782, [1205.1004].
- [3] T. Bringmann and C. Weniger, *Gamma ray signals from dark matter: Concepts, status and prospects*, *Physics of the Dark Universe* **1** (Nov., 2012) 194–217, [1208.5481].
- [4] R. Essig *et al.*, *Dark Sectors and New, Light, Weakly-Coupled Particles*, *ArXiv e-prints* (Oct., 2013) , [1311.0029].
- [5] L. E. Strigari, *Galactic searches for dark matter*, *Phys. Rept.* **531** (Oct., 2013) 1–88, [1211.7090].
- [6] K. Freese, M. Lisanti and C. Savage, *Colloquium: Annual modulation of dark matter*, *Reviews of Modern Physics* **85** (Oct., 2013) 1561–1581, [1209.3339].
- [7] T. R. Slatyer, *Indirect dark matter signatures in the cosmic dark ages. I. Generalizing the bound on  $s$ -wave dark matter annihilation from Planck results*, *Phys. Rev. D* **93** (Jan., 2016) 023527, [1506.03811].
- [8] H. Liu, T. R. Slatyer and J. Zavala, *Contributions to cosmic reionization from dark matter annihilation and decay*, *Phys. Rev. D* **94** (Sept., 2016) 063507, [1604.02457].
- [9] B. Carr, F. Kühnel and M. Sandstad, *Primordial black holes as dark matter*, *Phys. Rev. D* **94** (Oct., 2016) 083504, [1607.06077].
- [10] A. M. Green, *Astrophysical uncertainties on the local dark matter distribution and direct detection experiments*, *Journal of Physics G Nuclear Physics* **44** (Aug., 2017) 084001, [1703.10102].
- [11] Gaia Collaboration, T. Prusti, J. H. J. de Bruijne, A. G. A. Brown, A. Vallenari, C. Babusiaux *et al.*, *The Gaia mission*, *Astron. Astroph.* **595** (Nov., 2016) A1, [1609.04153].
- [12] and A. G. A. Brown, A. Vallenari, T. Prusti and J. H. J. de Bruijne *and*, *Gaia data release 2. summary of the contents and survey properties*, *Astron. Astroph.* (apr, 2018) , [1804.09365].
- [13] M. J. Reid, K. M. Menten, A. Brunthaler, X. W. Zheng, T. M. Dame, Y. Xu *et al.*, *Trigonometric Parallaxes of High Mass Star Forming Regions: The Structure and Kinematics of the Milky Way*, *Astrophys. J.* **783** (Mar., 2014) 130, [1401.5377].
- [14] T. Piffl, J. Binney, P. J. McMillan, M. Steinmetz, A. Helmi, R. F. G. Wyse *et al.*, *Constraining the Galaxy’s dark halo with RAVE stars*, *MNRAS* **445** (Dec., 2014) 3133–3151, [1406.4130].
- [15] J. Binney, *Self-consistent modelling of our galaxy with gaia data*, *ArXiv e-prints* (June, 2017) , [1706.01374].
- [16] D. G. Cerdeño, M. Fornasa, A. M. Green and M. Peiró, *How to calculate dark matter direct detection exclusion limits that are consistent with gamma rays from annihilation in the milky way halo*, *Phys. Rev. D* **94** (Aug., 2016) 043516, [1605.05185].
- [17] I. R. King, *The structure of star clusters. iii. some simple dynamical models*, *Astron. J.* **71** (Feb., 1966) 64.
- [18] J. Herzog-Arbeitman, M. Lisanti, P. Madau and L. Necib, *Empirical determination of dark matter velocities using metal-poor stars*, *Physical Review Letters* **120** (Jan., 2018) 041102, [1704.04499].
- [19] A. Pillepich, M. Vogelsberger, A. Deason, V. Rodriguez-Gomez, S. Genel, D. Nelson *et al.*, *Halo mass and assembly history exposed in the faint outskirts: the stellar and dark matter haloes of illustris galaxies*, *MNRAS* **444** (Oct., 2014) 237–249, [1406.1174].
- [20] J. Schaye, R. A. Crain, R. G. Bower, M. Furlong, M. Schaller, T. Theuns *et al.*, *The EAGLE project: simulating the evolution and assembly of galaxies and their environments*, *MNRAS* **446** (Jan., 2015) 521–554, [1407.7040].

- [21] T. Lacroix, A. Nunez, M. Stref, J. Lavallo and E. Nezri, *Predicting the dark matter velocity distribution from the Galactic content: tests against hydrodynamic cosmological simulations, in preparation* (2018) .
- [22] A. S. Eddington, *The distribution of stars in globular clusters*, *MNRAS* **76** (May, 1916) 572–585.
- [23] L. P. Osipkov, *Spherical systems of gravitating bodies with an ellipsoidal velocity distribution*, *Pisma v Astronomicheskii Zhurnal* **5** (Feb., 1979) 77–80.
- [24] D. Merritt, *Spherical stellar systems with spheroidal velocity distributions*, *Astron. J.* **90** (June, 1985) 1027–1037.
- [25] P. Ullio and M. Kamionkowski, *Velocity distributions and annual-modulation signatures of weakly-interacting massive particles*, *Journal of High Energy Physics* **3** (Mar., 2001) 049, [[hep-ph/0006183](#)].
- [26] J. D. Vergados and D. Owen, *New Velocity Distribution for Cold Dark Matter in the Context of the Eddington Theory*, *Astrophys. J.* **589** (May, 2003) 17–28, [[astro-ph/0203293](#)].
- [27] R. Catena and P. Ullio, *The local dark matter phase-space density and impact on WIMP direct detection*, *JCAP* **5** (May, 2012) 5, [[1111.3556](#)].
- [28] M. Pato, L. E. Strigari, R. Trotta and G. Bertone, *Taming astrophysical bias in direct dark matter searches*, *JCAP* **2** (Feb., 2013) 41, [[1211.7063](#)].
- [29] P. Bhattacharjee, S. Chaudhury, S. Kundu and S. Majumdar, *Deriving the velocity distribution of Galactic dark matter particles from the rotation curve data*, *Phys. Rev. D* **87** (Apr., 2013) 083525, [[1210.2328](#)].
- [30] N. Bozorgnia, R. Catena and T. Schwetz, *Anisotropic dark matter distribution functions and impact on WIMP direct detection*, *JCAP* **12** (Dec., 2013) 050, [[1310.0468](#)].
- [31] M. Fornasa and A. M. Green, *Self-consistent phase-space distribution function for the anisotropic dark matter halo of the Milky Way*, *Phys. Rev. D* **89** (Mar., 2014) 063531, [[1311.5477](#)].
- [32] J. Lavallo and S. Magni, *Making sense of the local Galactic escape speed estimates in direct dark matter searches*, *Phys. Rev. D* **91** (Jan., 2015) 023510, [[1411.1325](#)].
- [33] F. Ferrer and D. R. Hunter, *The impact of the phase-space density on the indirect detection of dark matter*, *JCAP* **9** (Sept., 2013) 5, [[1306.6586](#)].
- [34] D. R. Hunter, *Derivation of the anisotropy profile, constraints on the local velocity dispersion, and implications for direct detection*, *JCAP* **2** (Feb., 2014) 023, [[1311.0256](#)].
- [35] K. K. Boddy, J. Kumar, L. E. Strigari and M.-Y. Wang, *Sommerfeld-enhanced  $j$ -factors for dwarf spheroidal galaxies*, *Phys. Rev. D* **95** (June, 2017) 123008, [[1702.00408](#)].
- [36] M. Petac, P. Ullio and M. Valli, *On velocity-dependent dark matter annihilations in dwarf satellites*, *ArXiv e-prints* (Apr., 2018) , [[1804.05052](#)].
- [37] R. Catena and P. Ullio, *A novel determination of the local dark matter density*, *JCAP* **8** (Aug., 2010) 4, [[0907.0018](#)].
- [38] P. J. McMillan, *Mass models of the Milky Way*, *MNRAS* **414** (July, 2011) 2446–2457, [[1102.4340](#)].
- [39] P. J. McMillan, *The mass distribution and gravitational potential of the Milky Way*, *MNRAS* **465** (Feb., 2017) 76–94, [[1608.00971](#)].
- [40] J. Binney and S. Tremaine, *Galactic Dynamics: Second Edition*. Princeton University Press, 2008.

- [41] A. Ollongren, *Three-dimensional galactic stellar orbits*, *Bulletin of the Astronomical Institutes of the Netherlands* **16** (Oct., 1962) 241.
- [42] J. Binney, *The radius-dependence of velocity dispersion in elliptical galaxies*, *MNRAS* **190** (Mar., 1980) 873–880.
- [43] M. Hénon, *Numerical Experiments on the Stability of Spherical Stellar Systems*, *Astron. Astroph.* **24** (Apr., 1973) 229.
- [44] S. M. Kent and J. E. Gunn, *The dynamics of rich clusters of galaxies. I - The Coma cluster*, *Astron. J.* **87** (July, 1982) 945–971.
- [45] P. Cuddeford, *An analytic inversion for anisotropic spherical galaxies*, *MNRAS* **253** (Dec., 1991) 414–426.
- [46] N. W. Evans and J. H. An, *Distribution function of the dark matter*, *Phys. Rev.* **D73** (2006) 023524, [[astro-ph/0511687](#)].
- [47] R. Wojtak, E. L. Lokas, G. A. Mamon, S. Gottlöber, A. Klypin and Y. Hoffman, *The distribution function of dark matter in massive haloes*, *MNRAS* **388** (Aug., 2008) 815–828, [[0802.0429](#)].
- [48] J. L. Sanders and J. Binney, *A review of action estimation methods for galactic dynamics*, *MNRAS* **457** (Apr., 2016) 2107–2121, [[1511.08213](#)].
- [49] T. Piffl, Z. Penoyre and J. Binney, *Bringing the Galaxy’s dark halo to life*, *MNRAS* **451** (July, 2015) 639–650, [[1502.02916](#)].
- [50] J. Binney and T. Piffl, *The distribution function of the Galaxy’s dark halo*, *MNRAS* **454** (Dec., 2015) 3653–3663, [[1509.06877](#)].
- [51] D. R. Cole and J. Binney, *A centrally heated dark halo for our Galaxy*, *MNRAS* **465** (Feb., 2017) 798–810, [[1610.07818](#)].
- [52] M. Portail, O. Gerhard, C. Wegg and M. Ness, *Dynamical modelling of the galactic bulge and bar: the Milky Way’s pattern speed, stellar and dark matter mass distribution*, *MNRAS* **465** (Feb., 2017) 1621–1644, [[1608.07954](#)].
- [53] T. Piffl, C. Scannapieco, J. Binney, M. Steinmetz, R.-D. Scholz, M. E. K. Williams et al., *The RAVE survey: the Galactic escape speed and the mass of the Milky Way*, *Astron. Astroph.* **562** (Feb., 2014) A91, [[1309.4293](#)].
- [54] L. L. Watkins, N. W. Evans and J. H. An, *The masses of the Milky Way and Andromeda galaxies*, *MNRAS* **406** (July, 2010) 264–278, [[1002.4565](#)].
- [55] V. Springel and S. D. M. White, *Tidal tails in cold dark matter cosmologies*, *MNRAS* **307** (July, 1999) 162–178, [[astro-ph/9807320](#)].
- [56] S. Kazantzidis, J. Magorrian and B. Moore, *Generating Equilibrium Dark Matter Halos: Inadequacies of the Local Maxwellian Approximation*, *Astrophys. J.* **601** (Jan., 2004) 37–46, [[astro-ph/0309517](#)].
- [57] R. V. D. R. Woolley, *A study of the equilibrium of globular clusters*, *MNRAS* **114** (1954) 191.
- [58] R. V. D. R. Woolley and D. A. Robertson, *Studies in the equilibrium of globular clusters (ii)*, *MNRAS* **116** (1956) 288.
- [59] I. King, *The structure of star clusters. I. an empirical density law*, *Astron. J.* **67** (Oct., 1962) 471.
- [60] R. W. Michie, *On the distribution of high energy stars in spherical stellar systems*, *MNRAS* **125** (1963) 127.
- [61] R. W. Michie and P. H. Bodenheimer, *The dynamics of spherical stellar systems, ii*, *MNRAS* **126** (1963) 269.

- [62] L. M. Widrow and J. Dubinski, *Equilibrium Disk-Bulge-Halo Models for the Milky Way and Andromeda Galaxies*, *Astrophys. J.* **631** (Oct., 2005) 838–855, [[astro-ph/0506177](#)].
- [63] N. E. Drakos, J. E. Taylor and A. J. Benson, *The phase-space structure of tidally stripped haloes*, *MNRAS* **468** (June, 2017) 2345–2358, [[1703.07836](#)].
- [64] L. E. Strigari, C. S. Frenk and S. D. M. White, *Dynamical models for the sculptor dwarf spheroidal in a  $\Lambda$ cdm universe*, *Astrophys. J.* **838** (Apr., 2017) 123.
- [65] V. S. Berezinsky, V. I. Dokuchaev and Y. N. Eroshenko, *Small-scale clumps of dark matter*, *Physics Uspekhi* **57** (Jan., 2014) 1–36, [[1405.2204](#)].
- [66] M. Stref and J. Lavalle, *Modeling dark matter subhalos in a constrained galaxy: Global mass and boosted annihilation profiles*, *Phys. Rev. D* **95** (Mar., 2017) 063003, [[1610.02233](#)].
- [67] J.-H. Choi, M. D. Weinberg and N. Katz, *The dynamics of satellite disruption in cold dark matter haloes*, *MNRAS* **400** (Dec., 2009) 1247–1263, [[0812.0009](#)].
- [68] L. M. Widrow, *Distribution Functions for Cuspy Dark Matter Density Profiles*, *Astrophys. J. Suppl. Series* **131** (Nov., 2000) 39–46, [[astro-ph/0003302](#)].
- [69] L. Ciotti and S. Pellegrini, *Self-consistent two-component models of elliptical galaxies*, *MNRAS* **255** (Apr., 1992) 561–571.
- [70] L. Ciotti, *The Analytical Distribution Function of Anisotropic Two-Component Hernquist Models*, *Astrophys. J.* **471** (Nov., 1996) 68, [[astro-ph/9605084](#)].
- [71] J. H. An and N. W. Evans, *A Cusp Slope-Central Anisotropy Theorem*, *Astrophys. J.* **642** (May, 2006) 752–758, [[astro-ph/0511686](#)].
- [72] L. Ciotti and L. Morganti, *How general is the global density slope-anisotropy inequality?*, *MNRAS* **408** (Oct., 2010) 1070–1074, [[1006.2344](#)].
- [73] V. A. Antonov, *Solution of the problem of stability of stellar system emden’s density law and the spherical distribution of velocities*, in *Vestnik Leningradskogo Universiteta, Leningrad: University, 1962*, 1962, <http://adsabs.harvard.edu/abs/1962spss.book.....A>.
- [74] N. R. Lebovitz, *On Schwarzschild’s Criterion for the Stability of Gaseous Masses.*, *Astrophys. J.* **142** (July, 1965) 229.
- [75] D. Lynden-Bell and R. Wood, *The gravo-thermal catastrophe in isothermal spheres and the onset of red-giant structure for stellar systems*, *MNRAS* **138** (1968) 495.
- [76] J.-P. Doremus, M. R. Feix and G. Baumann, *Stability of encounterless spherical stellar systems*, *Phys. Rev. Lett.* **26** (Mar., 1971) 725–728.
- [77] H. E. Kandrup and J. F. Sygnet, *A simple proof of dynamical stability for a class of spherical clusters*, *Astrophys. J.* **298** (Nov., 1985) 27–33.
- [78] J. P. Doremus, G. Baumann and M. R. Feix, *Stability of a Self Gravitating System with Phase Space Density Function of Energy and Angular Momentum*, *Astron. Astroph.* **29** (Dec., 1973) 401.
- [79] V. A. Antonov, *Solution of the problem of stability of a stellar system with emden’s density law and a spherical distribution of velocities*, in *Structure and Dynamics of Elliptical Galaxies* (P. T. de Zeeuw, ed.), vol. 127 of *IAU Symposium*, p. 531, 1987, <http://adsabs.harvard.edu/abs/1987IAUS..127..531A>.
- [80] J. Perez and J.-J. Aly, *Stability of spherical stellar systems - i. analytical results*, *MNRAS* **280** (June, 1996) 689–699, [[astro-ph/9511103](#)].
- [81] G. Rein and Y. Guo, *Stable models of elliptical galaxies*, *MNRAS* **344** (Oct., 2003) 1296–1306, [[astro-ph/0203274](#)].

- [82] L. Maréchal and J. Perez, *Radial orbit instability as a dissipation-induced phenomenon*, *MNRAS* **405** (July, 2010) 2785–2790, [[1003.2354](#)].
- [83] D. Merritt and L. A. Aguilar, *A numerical study of the stability of spherical galaxies*, *MNRAS* **217** (Dec., 1985) 787–804.
- [84] J. Barnes, J. Goodman and P. Hut, *Dynamical instabilities in spherical stellar systems*, *Astrophys. J.* **300** (Jan., 1986) 112–131.
- [85] A. Meza and N. Zamorano, *Numerical Stability of a Family of Osipkov-Merritt Models*, *Astrophys. J.* **490** (Nov., 1997) 136–142, [[astro-ph/9707004](#)].
- [86] J. D. Lewin and P. F. Smith, *Review of mathematics, numerical factors, and corrections for dark matter experiments based on elastic nuclear recoil*, *Astroparticle Physics* **6** (Dec., 1996) 87–112.
- [87] W. H. Press and D. N. Spergel, *Capture by the sun of a galactic population of weakly interacting massive particles*, *Astrophys. J.* **296** (Sept., 1985) 679–684.
- [88] A. Gould, *Weakly interacting massive particle distribution in and evaporation from the sun*, *Astrophys. J.* **321** (Oct., 1987) 560–570.
- [89] P. Salati and J. Silk, *A stellar probe of dark matter annihilation in galactic nuclei*, *Astrophys. J.* **338** (Mar., 1989) 24–31.
- [90] A. Bouquet and P. Salati, *Life and death of cosmions in stars*, *Astron. Astroph.* **217** (June, 1989) 270–282.
- [91] A. Bouquet and P. Salati, *Dark matter and the suppression of stellar core convection*, *Astrophys. J.* **346** (Nov., 1989) 284–288.
- [92] C. Kouvaris, *Wimp annihilation and cooling of neutron stars*, *Phys. Rev. D* **77** (Jan., 2008) 023006, [[0708.2362](#)].
- [93] G. Bertone and M. Fairbairn, *Compact stars as dark matter probes*, *Phys. Rev. D* **77** (Feb., 2008) 043515, [[0709.1485](#)].
- [94] K. Griest, *Galactic microlensing as a method of detecting massive compact halo objects*, *Astrophys. J.* **366** (Jan., 1991) 412–421.
- [95] A. M. Green, *Astrophysical uncertainties on stellar microlensing constraints on multi-Solar mass primordial black hole dark matter*, *Journal of Physics G Nuclear Physics* **44** (Aug., 2017) 084001, [[1705.10818](#)].
- [96] J. Hisano, S. Matsumoto, M. M. Nojiri and O. Saito, *Nonperturbative effect on dark matter annihilation and gamma ray signature from the galactic center*, *Phys. Rev. D* **71** (Mar., 2005) 063528, [[hep-ph/0412403](#)].
- [97] P. Gondolo and G. Gelmini, *Cosmic abundances of stable particles: improved analysis.*, *Nuclear Physics B* **360** (Aug., 1991) 145–179.
- [98] H. Zhao, *Analytical models for galactic nuclei*, *MNRAS* **278** (Jan., 1996) 488–496, [[astro-ph/9509122](#)].